

# The Assembly of Supermassive Black Holes at High Redshifts

Takamitsu Tanaka and Zoltán Haiman

*Department of Astronomy, Columbia University, 550 W120th St., New York, NY 10027*

## ABSTRACT

The supermassive black holes (SMBHs) massive enough ( $\gtrsim \text{few} \times 10^9 M_\odot$ ) to power the bright redshift  $z \approx 6$  quasars observed in the Sloan Digital Sky Survey (SDSS) are thought to have assembled by mergers and/or gas accretion from less massive “seed” BHs. If the seeds are the  $\sim 10^2 M_\odot$  remnant BHs from the first generation of stars, they must be in place well before redshift  $z = 6$ , and must avoid being ejected from their parent proto-galaxies by the large (several  $\times 10^2 \text{ km s}^{-1}$ ) kicks they suffer from gravitational-radiation induced recoil during mergers with other BHs. We simulate the SMBH mass function at redshift  $z > 6$  using dark matter (DM) halo merger trees, coupled with a prescription for the halo occupation fraction, accretion histories, and radial recoil trajectories of the growing BHs. Our purpose is (i) to map out plausible scenarios for successful assembly of the  $z \approx 6$  quasar BHs by exploring a wide region of parameter space, and (ii) to predict the rate of low-frequency gravitational wave events detectable by the *Laser Interferometer Space Antenna (LISA)* for each such scenario. Our main findings are as follows: (1)  $\sim 100 M_\odot$  seed BHs can grow into the SDSS quasar BHs without super-Eddington accretion, but only if they form in minihalos at  $z \gtrsim 30$  and subsequently accrete  $\gtrsim 60\%$  of the time; (2) the scenarios with optimistic assumptions required to explain the SDSS quasar BHs overproduce the mass density in lower-mass ( $\text{few} \times 10^5 M_\odot \lesssim M_{\text{bh}} \lesssim \text{few} \times 10^7 M_\odot$ ) BHs by a factor of  $10^2 - 10^3$ , unless seeds stop forming, or accrete at a severely diminished rates or duty cycles (e.g. due to feedback), at  $z \lesssim 20 - 30$ . We also present several successful assembly models and their *LISA* detection rates, including a “maximal” model that gives the highest rate ( $\sim 30 \text{ yr}^{-1}$  at  $z = 6$ ) without overproducing the total SMBH density.

*Subject headings:* cosmology: theory – galaxies: formation – quasars: general – black hole physics – accretion

## 1. Introduction

The discovery of bright quasars at redshifts  $z \gtrsim 6$  in the Sloan Digital Sky Survey (SDSS) implies that black holes (BHs) as massive as several  $\times 10^9 M_\odot$  were already assembled when the age of the universe was less than  $\approx 1$  Gyr (see the recent review by Fan 2006). These objects are among the oldest detected discrete sources of radiation in the Universe. The likelihood that all of these quasars are significantly magnified by gravitational lensing, without producing detectable multiple images (Richards et al. 2004), is exceedingly small (Keeton et al. 2005), and if their luminosities are powered by accretion at or below the Eddington rate, the central objects must be  $\sim 10^9 M_\odot$  supermassive black holes (SMBHs). In particular, the quasar SDSS J1148+5251 (Fan et al. 2003, 2001) is likely to be powered by a SMBH with a mass of  $\approx 10^{9.5} M_\odot$  (Willott et al. 2003).

The mechanism by which such massive BHs formed within 1 Gyr after the Big Bang remains poorly understood. Generically, these SMBHs are thought to have assembled by mergers with other BHs and/or by gas accretion<sup>1</sup> onto less massive BHs. If the first (“seed”) BHs are the  $\sim 10^2 M_\odot$  remnant BHs of the first generation of stars (e.g. Heger et al. 2003), they must be in place well before redshift  $z = 6$ . If accretion onto BHs is limited at the Eddington rate with radiative efficiency  $\epsilon$ , defined as the fraction of the rest mass energy of matter falling onto the BH that is released as radiation, then  $1 - \epsilon$  of the matter is accreted and the growth of the BH mass  $m$  is given by

$$\frac{d \ln m}{dt} = \frac{1 - \epsilon}{\epsilon} \frac{4\pi G \mu m_{\text{p}}}{\sigma_e c}, \quad (1)$$

where  $G$  is the gravitational constant,  $c$  is the speed of light,  $\mu \approx 1.15$  is the mean atomic weight per electron for a primordial gas, and  $\sigma_e$  is the Thompson electron cross section. The e-folding time scale for mass growth is  $t_{\text{Edd}} \approx 4.4 \times 10^7$  yr for  $\epsilon = 0.1$ . In the concordance cosmological model (see below) the time elapsed between redshifts  $z = 30$  (when the first seeds may form) and  $z = 6.4$  (the redshift of the most distant quasar) is  $\approx 0.77$  Gyr, allowing for a mass growth by a factor of  $\approx 10^{7.7}$ . Therefore, individual  $\sim 100 M_\odot$  seeds can grow into the SDSS quasar BHs through gas accretion alone, provided the accretion is uninterrupted at close to the Eddington rate and  $\epsilon \lesssim 0.1$ . A higher efficiency and/or a lower time-averaged accretion rate will require many seed BHs to merge together; the number of required mergers increases exponentially for lower time-averaged accretion rates.

The discovery of the bright quasars at  $z \gtrsim 6$  were followed by the first successful numerical calculations in full general relativity of the coalescence of a BH binary and the

---

<sup>1</sup>In this paper, “accretion” onto BHs should be assumed to mean gas accretion, unless otherwise noted.

corresponding emission of gravitational waves (GWs) (Pretorius 2005; Campanelli et al. 2006; Baker et al. 2006). These calculations also confirmed a result previously known from post-Newtonian (Kidder 1995) and perturbation-theory treatments (Favata et al. 2004, Schnittman & Buonanno 2007): the coalesced product receives a large center-of-mass recoil imparted by the net linear momentum accumulated by the asymmetric gravitational wave emission (see Schnittman et al. 2008 for a recent detailed discussion of the physics of the recoil, and for further references). Typical velocities for this gravitational recoil (or “kick”) are in excess of  $\sim 100 \text{ km s}^{-1}$ . This is likely more than sufficient to eject the BHs residing in the low-mass protogalaxies in the early Universe, since the escape velocities from the DM halos of these galaxies are only a few  $\text{km s}^{-1}$ .

Several recent works have studied the role of gravitational kicks as an impediment to merger-driven modes of SMBH assembly. Simple semi-analytic models show that if every merger resulted in a kick large enough to remove the seed BHs from halos with velocity dispersions up to  $\approx 50 \text{ km s}^{-1}$ , then super-Eddington accretion would be required to build SMBHs of the required mass in the available time (Haiman 2004; Shapiro 2005). Monte-Carlo merger tree models that exclude kicks entirely (Bromley et al. 2004) or which include a distribution of kick velocities extending to low values (e.g. Yoo & Miralda-Escudé 2004 [hereafter YM04]; Volonteri & Rees 2006 [hereafter VR06]) give a slightly more optimistic picture, showing that if seed BHs form in most minihalos in the early Universe, and especially if ejected seeds are rapidly replaced by new seeds (YM04), then SMBH assembly is just possible before  $z \approx 6$  without exceeding the Eddington accretion rate. These works are encouraging steps toward demonstrating that there are plausible physical models that lead to the timely assembly of SMBHs massive enough to power the  $z > 6$  SDSS quasars.

At present, we have no direct observational constraints on SMBH assembly at  $z > 6$ , and there is, in principle, a large range of “physically plausible” possibilities. The *Laser Interferometer Space Antenna* (*LISA*) is expected to be able to detect mergers of SMBHs in the mass range  $\sim (10^4\text{--}10^7) M_{\odot}/(1+z)$  out to  $z \sim 30$ , and to extract binary spins and BH masses with high precision up to  $z \sim 10$  (Vecchio 2004; Lang & Hughes 2006, 2007). It is also likely that by the time *LISA* is operational, there will be additional independent constraints on the demography of high-redshift SMBHs. It is therefore a useful exercise to calculate the expected *LISA* event rate from high-redshift SMBH mergers (e.g. Wyithe & Loeb 2003; Sesana et al. 2004, 2005, 2007) in a range of plausible models. Note that published estimates (Menou et al. 2001, Heger et al. 2003, Menou 2003, Haehnelt 2003, Wyithe & Loeb 2003, Sesana et al. 2004, Islam et al. 2004, Koushiappas & Zentner 2006, Micic et al. 2007, Lippai et al. 2008, Arun et al. 2008) for the *LISA* event rate, even at lower redshifts, vary by orders of magnitude, from  $\sim 1$  to as high as  $\sim 10^4 \text{ yr}^{-1}$ ; there is a large range even among models that explicitly fit the evolution of the quasar luminosity function (12). A related

open question is to what degree the *LISA* data stream can help pinpoint the actual SMBH assembly scenario. One aim of this paper is to understand the model degeneracies that can lead to similar *LISA* data streams. Another is to explore as much as possible the full variety of *LISA* event rates arising from various “physically plausible” assembly models.

The physical factors that determine the growth of SMBHs at high redshift fall broadly into four categories: (1) the properties of the initial seed BHs, such as their redshift, mass, and abundance; (2) the time-averaged gas accretion rate of individual seeds; (3) the merger rates of BHs; and (4) effects governing the fate of gravitationally kicked BHs. The first category determines the number and mass of seed BHs available for assembly, and depends primarily on the behavior of gas in the host DM halos, and the mass and metallicity of the first stars. The second category measures the subsequent growth through accretion, and depends on the availability of fuel over the Hubble time, and its ability to shed angular momentum and accrete onto the BH. The third category is a combination of the halo merger rate, the rarity of seeds, and the timescale for the formation, orbital decay, and ultimate coalescence of a SMBH binary. Finally, the recoil velocity of the coalesced binary is determined by the mass ratio and spin vectors of the BHs, and its subsequent orbit – and whether it is retained or ejected before the next merger – will be determined by the overall depth of the gravitational potential of the DM host halo, and on the spatial distribution of gas and DM in the central region of the halo, which determine drag forces on the kicked BH.

Our approach to model the above effects closely follows those in earlier works (e.g. YM04; Bromley et al. 2004; Sesana et al. 2004; VR06): we use Monte Carlo merger trees to track the hierarchical growth of DM halos, and a simple semi-analytical model to follow the growth and dynamics of BHs. We expand over earlier works by adding an explicit calculation of the orbits of kicked BHs, and self-consistently include their corresponding time-dependent accretion rate. Additionally, we extend the merger tree to redshifts beyond  $z > 40$ , and we examine a large range of different models. For each set of model parameters, we apply our “tree-plus-orbits” algorithm to the entire halo population at  $z \approx 6$  to construct a full population of SMBHs at this redshift, and calculate physical quantities of interest: the mass function, the SMBH-to-halo mass ratio, the fraction of DM halos hosting SMBHs, and the expected detection rate of SMBH mergers by *LISA*.

This algorithm assembles SMBHs through simple prescriptions of the aforementioned four categories of physical contributions to SMBH formation. We model the seed population by assuming that some fraction  $f_{\text{seed}}$  of DM halos reaching a threshold virial temperature  $T_{\text{seed}}$  forms a Pop III remnant BH. In-between mergers, the BHs are assumed to accrete gas at a rate of  $f_{\text{duty}}$  times the Eddington rate  $\dot{m}_{\text{Edd}} \equiv (1 - \epsilon)/\epsilon \times L_{\text{Edd}}/c^2$ . Here  $f_{\text{duty}}$  should be interpreted as the mean gas accretion rate (averaged over time-scales comparable

to the Hubble time) in units of the Eddington rate. Note that this prescription makes no distinction between episodic accretion near the Eddington rate during a fraction  $f_{\text{duty}}$  of the time (with no accretion in-between), and constant accretion at all times at a fraction  $f_{\text{duty}}$  of the Eddington rate. We assume that the mergers of BH binaries closely follow the mergers of their host halos (but allow for a delay in the latter due to dynamical friction). Finally, we simulate the orbits of recoiling BHs under different assumptions about the baryon density profile and binary spin orientation. We discuss the relative importance of assembly model parameters on the final SMBH mass function and the *LISA* data stream, and ask whether *LISA* will be able to uniquely determine the underlying assembly model from data. We also examine several variants of the above scenario, in which (i) the seed BHs are massive,  $\sim 10^5 M_\odot$ , and formed from the super-Eddington accretion of a collapsed gaseous core; (ii) the DM halo is initially devoid of gas when the seed BHs is formed; (iii) seed BHs stop forming below some redshift; and (iv) models which maintain the so-called  $M_{\text{bh}} - \sigma$  relation between BH mass and (halo) velocity dispersion (Ferrarese & Merritt 2000; Gebhardt et al. 2000) at all redshifts.

This paper is organized as follows. In § 2, we detail our methodology by describing our assumptions, the assembly algorithm, including the prescriptions of the aforementioned physical effects, and the different assembly scenarios we consider. We present and discuss our main results in § 3. In § 4, we summarize our most important results, and comment on future prospects to understand SMBH assembly at high redshift. To keep our notation as simple as possible, throughout this paper the capital  $M$  will be used to denote halo masses, and  $m$  will refer to BH masses. In this paper, we adopt a  $\Lambda$ CDM cosmology, with the parameters inferred by Komatsu et al. (2008) using the five-year data from the *Wilkinson Microwave Anisotropy Probe* (*WMAP5*):  $\Omega_{\text{CDM}} = 0.233$ ,  $\Omega_b = 0.046$ ,  $\Omega_\Lambda = 0.721$ ,  $h = 0.70$ , and  $\sigma_8 = 0.82$ . We use  $n_s = 1$  for the scalar index.

## 2. Assumptions and Model Description

Our strategy is as follows: (1) We use Monte Carlo merger trees to construct the hierarchical merger history of DM halos with masses  $M > 10^8 M_\odot$  at redshift  $z = 6$ , i.e. those that can host SMBHs of mass  $m \gtrsim 10^5 M_\odot$ ; (2) We insert seed BHs of mass  $m_{\text{seed}}$  into the tree in some fraction  $f_{\text{seed}}$  of halos that reach a threshold temperature  $T_{\text{seed}}$ ; (3) We follow the subsequent BH assembly history by allowing the BHs to grow by gas accretion in-between mergers, and by calculating the orbit and accretion history of each recoiling BH in its host halo. We assume that BHs add their masses linearly upon merging, and ignore mass losses due to gravitational radiation, as these losses never accumulate to significant levels, even through

repeated mergers (Menou & Haiman 2004). We prescribe spin distributions of the BHs and gas distributions within their host halos. We repeat this procedure for different mass bins of the halo mass function, until we have a statistically robust sample to represent the global SMBH mass function at redshift  $z = 6$  to an accuracy of a factor of two. We also record the BH binary mergers whose masses lie within the mass range  $\sim (10^4\text{--}10^7) M_\odot/(1+z)$ , corresponding roughly to *LISA*'s sensitivity range.

## 2.1. The Merger Tree

We construct DM merger trees based on the algorithm by Volonteri et al. (2003), which allows only binary mergers. Similar numerical algorithms (e.g. Somerville & Kolatt 1999; Cole et al. 2000) give somewhat different results, as have been discussed recently by Zhang et al. (2008). We will not reproduce the Volonteri et al. (2003) recipe here in full; instead we present a brief review. We take the extended Press-Schechter (EPS) mass function (Press & Schechter 1974, Lacey & Cole 1993),

$$\frac{dN}{dM} = \frac{1}{\sqrt{2\pi}} \frac{M_0}{M} \frac{d\sigma_M^2}{dM} \frac{\delta_c(z) - \delta_c(z_0)}{(\sigma_M^2 - \sigma_{M_0}^2)^{3/2}} \exp \left\{ -\frac{1}{2} \frac{[\delta_c(z) - \delta_c(z_0)]^2}{\sigma_M^2 - \sigma_{M_0}^2} \right\}, \quad (2)$$

which gives for a parent halo of mass  $M_0$  at redshift  $z_0$  the number of progenitor halos in the range  $M \pm dM/2$  at a higher redshift  $z$ . Here  $\sigma_M$  is the amplitude of the linear matter fluctuations at redshift  $z = 0$ , smoothed by a top hat window function whose scale is such that the enclosed mass at the mean density is  $M$  (computed using the fitting formula for the transfer function provided in Eisenstein & Hu 1999), and  $\delta_c$  is the redshift-dependent critical overdensity for collapse. We take the limit as  $\Delta z \equiv z - z_0 \rightarrow 0$ :

$$\frac{dN}{dM} = \frac{1}{\sqrt{2\pi}} \frac{M_0}{M} \frac{d\sigma_M^2}{dM} (\sigma_M^2 - \sigma_{M_0}^2)^{-3/2} \frac{d\delta_c}{dz} \Delta z. \quad (3)$$

The two advantages of taking this limit are that (i) by linearizing the expression, the  $z$ - and  $M$ -dependences separate, allowing a tabulation as functions of the parent & progenitor halo mass, and (ii) separating  $\Delta z$  allows for a simple algorithm for adaptive timesteps to make sure that fragmentations produce binaries at most (no triplets).

For a parent halo of mass  $M_p$  after a small step  $\Delta z$ , the mean number of “minor” fragments in the mass range  $M_{\text{lo}} < m < M_p/2$  is given by

$$N_p = \int_{M_{\text{lo}}}^{M_p/2} \frac{dN}{dM} dM \propto \Delta z. \quad (4)$$

We choose  $\Delta z$  adaptively such that  $N_p \ll 1$ , which ensures that multiple fragmentations are unlikely in a given single time step. We place a lower limit of  $10^{-3}$  (in redshift units) for the timestep to keep computation times manageable. The integral in Equation (4) diverges as  $M_{\text{lo}} \rightarrow 0$ , making it computationally prohibitive to compute the merger history of arbitrarily small halos. To avoid this problem, all progenitors below a fixed mass resolution  $M_{\text{res}}$  are considered jointly as accreted mass and not tracked individually. Any progenitor with  $M < M_{\text{res}}(z)$  is thus discarded from the tree and its prior history is disregarded. For our calculations, we choose  $M_{\text{res}}(z)$  to be the mass corresponding to a virial temperature of 1200K, corresponding to  $M_{\text{res}} \sim 4.7 \times 10^5 M_{\odot}$  at  $z = 40$  and  $3.4 \times 10^6 M_{\odot}$  at  $z = 10$ . Theoretical studies have concluded that Pop III stars can start forming at lower virial temperatures,<sup>2</sup> but numerical considerations have forced us to adopt a somewhat larger threshold. We do not impose an explicit upper redshift limit, and we run the tree until our halos at  $z = 6$  are entirely broken up into progenitors with  $M < M_{\text{res}}$ . As a check on our Monte-Carlo merger tree algorithm, in Figure 1, we present the progenitor mass functions of a  $10^{12} M_{\odot}$ ,  $z_0 = 6$  parent halo at redshifts of  $z = 8, 13, 21$  and  $34$ , together with the Poisson errors of the merger tree output and the predictions from the EPS conditional mass function (eq. 2). Our merger tree results are consistent with the EPS conditional mass function up to redshift  $z \approx 40$ , with agreement within a factor of two for most mass bins and redshift values. In particular, the numerical mass function agrees well with the EPS prediction for the low-mass progenitors, even at very high redshift, but the higher-mass progenitors are under-predicted by a factor of up to two. We note that Cole et al. (2000) used a numerical algorithm similar to the one we adopted, to construct a halo merger-tree. As discussed in Zhang et al. (2008), that algorithm results in a similar inaccuracy.

## 2.2. The Initial Black Hole Population

The conditions under which the first black holes form are highly uncertain, though numerical simulations (Abel et al. 2002, O’Shea & Norman 2007) do provide useful indications. We parametrize our ignorance in terms of a seeding fraction, such that a fraction  $f_{\text{seed}}$  of all halos reaching the critical virial temperature  $T_{\text{seed}}$  form a seed BH. There are physical mechanisms that make a low seeding fraction plausible: the first stars may form only in rare,

---

<sup>2</sup>Haiman et al. (1996), Tegmark et al. (1997) and Machacek et al. (2001) suggest a threshold virial temperature of  $\sim 400\text{K}$  for collapse. In their recent high-resolution numerical simulations, O’Shea and Norman (2007) find star formation in halos of masses  $(1.5 - 7) \times 10^5 M_{\odot}$  between  $19 < z < 33$ , with no significant redshift dependence on the mass scatter. These values correspond to virial temperatures of  $260 - 1300\text{K}$ .

baryon-rich overdense regions with unusually low angular momentum, and seed remnants may receive ejecting kicks from collapse asymmetry mechanisms similar to those responsible for high-velocity pulsars. Furthermore, radiative and other feedback processes may prohibit  $\text{H}_2$ -formation, cooling, and star-formation in the majority of low-mass minihalos at high redshift (e.g. Haiman, Rees & Loeb 1997; Mesinger et al. 2006). Since the *LISA* event rate, especially at the earliest epochs, will depend primarily on the abundance of BHs present, it is highly sensitive to the seeding function.

We choose two fiducial seeding models, the first with  $T_{\text{seed}} = 1200\text{K}$  (the minimum value required for metal-free molecular line cooling and star formation) for a Pop-III remnant seed BH with  $m_{\text{seed}} = 100M_{\odot}$ . The second model has  $T_{\text{seed}} = 1.5 \times 10^4\text{K}$  and  $m_{\text{seed}} = 10^5M_{\odot}$ , inspired by the “direct collapse” models of more massive BHs from the central gas in halos with a deep enough potential to allow atomic cooling (Oh & Haiman 2002; Bromm & Loeb 2003; Volonteri & Rees 2005; Begelman et al. 2006; Spaans & Silk 2006; Lodato & Natarajan 2006). If Eddington accretion is the main mode of growth, then we do not expect the choice of seed mass for each type of model to qualitatively affect our results, other than the obvious linear scaling of the overall BH mass function with the initial seed mass. Only the binary mass ratios affect recoil magnitudes, and the subsequent orbital dynamics depends minimally on the BH mass.

### 2.3. Baryonic and Dark Matter Halo Profiles

The DM profile for the earliest halos is found to be similar to the NFW (Navarro, Frenk and White 1997) profile of lower-redshift, more massive DM halos (Abel et al. 2000; Bromm et al. 2002; Yoshida et al. 2003). However, the composition and spatial distribution of the baryons, at the time when the seed BH appears in these halos, is poorly understood, and is unconstrained by observations. This is unfortunate, since these quantities play a pivotal role in determining the orbital dynamics and growth rate of a recoiling BH.

A steep profile with a cusp will retain BHs more effectively, owing both to a deeper gravitational potential well and a larger dynamical drag force at the halo center. The baryon distribution will also determine the accretion history of the central BH by determining the accretion rate as the BH rests near the halo’s potential center, or as it oscillates in a damped orbit through the halo following a recoil displacement event.

In addition, whether the baryons are gaseous or stellar has nontrivial consequences, owing to the difference in the dynamical friction force between the two cases. A collisional medium provides a greater dynamical friction force than a stellar or DM medium with



the same density profile (Ostriker 1999; Escala et al. 2004). Because of the difference in the drag force, an environment dominated by gas, and not by stars (or dark matter), has several possible consequences on BHs: (1) binaries coalesce more rapidly; (2) a BH recoiling in gas has a higher likelihood of being retained in its parent halo; and (3) any “vagrant” BH that is displaced from the baryon-rich center of the gravitational potential of its host halo takes less time to return there, reducing episodes of suppressed accretion. In three-dimensional simulations of star-formation in metal-free minihalos suggest that star-formation is inefficient, with either a single star, or at most a few stars, forming at the center of the halo (Abel et al. 2000; Bromm et al. 2002; Yoshida et al. 2003, 2008). Since in the context of this paper we are concerned with the pre-reionization Universe, we work with the assumption that stars are rare before  $z \gtrsim 6$  and that the baryons in our halos are mostly gaseous.

We model each galaxy as a spherically symmetric mass distribution with two components: a DM halo with an NFW profile, and a superimposed baryonic component. Previous studies on this subject (see e.g. Volonteri et al. 2003; Madau & Quataert 2004) have often assumed a non-collisional singular isothermal sphere (SIS) profile for the mass distribution. This is justified if the gas does not cool significantly below the virial temperature of the DM halo, and if it has little angular momentum (so that it is supported thermally, rather than by rotation). In most halos whose virial temperature is above  $10^4\text{K}$ , this assumption is less justified, and a disk may form at the core of the DM halo (Oh & Haiman 2002). The direct collapse scenario in Begelman et al. (2006) and also VR06 adopt such a “fat disk” configuration. However, the central densities of such disks are within the range of our adopted spherical profiles. For simplicity, here we only consider three different prescriptions for spherical gas distribution. Our fiducial gas profile is a cuspy,  $\rho \propto r^{-2.2}$  power law, where we have taken the power-law index of 2.2 as suggested by numerical simulations of the first star-forming minihalos (Machacek et al. 2001). This profile is established in halos that are able to cool their gas via  $\text{H}_2$ , and describes the gas distribution at the time of the first star-formation.

It is possible, however, that the typical seed BHs are surrounded by a very different gas distribution, at the time of their formation. First, the progenitor Pop-III stars of the first seed BHs are here assumed to form in DM halos of mass  $\sim 10^{5-6}M_\odot$ . The UV radiation from the star will photo-heat, and easily blow out most of the gas from low-mass minihalos, even before the star collapses to leave behind a seed BH (e.g. Whalen et al. 2004). In this case, the remnant BH will find itself in a DM halo devoid of gas, and can only start accreting once a merger with another, gas-rich halo has taken place, or until the parent halo has accreted enough mass to replenish its gas (e.g. Alvarez et al. 2008). We therefore make the simple assumption that *no* gas is present, until the minihalo containing the newly-formed seed BH

merges with another halo, or grows sufficiently – assumed here to be a factor of 10 – in mass. However, we will examine the consequences of this assumption below, by performing runs without such a blow-out phase.

Second, as mentioned above, feedback processes may prohibit  $\text{H}_2$ -formation and cooling in the majority of the low-mass minihalos (e.g. Haiman, Rees & Loeb 1997; Mesinger et al. 2006). The gas in such minihalos remains nearly adiabatic, and can not contract to high densities. To allow for this possibility, we will study a variant for the effective gas profile. Specifically, we adopt the gas distribution in these halos by the truncated isothermal sphere (TIS) profile proposed in Shapiro et al. (1999), which has an  $r^{-2}$  profile at large radii, but has a flat core at the center owing to the central gas pressure. The density profile is normalized (here, and also in our fiducial gas profile above) such that the total baryon-to-DM mass ratio inside the virial radius  $r_{200}$  equals the cosmological value. Both the DM and the baryonic components are assumed to extend out to  $10r_{\text{vir}}$ , at which point the density falls to the background value. This is consistent with infall-collapse models of Barkana (2004).

## 2.4. Mergers of Dark Matter Halos and Black Holes

We next have to make important assumptions about the treatment of mergers between dark matter halos and their resident BHs.

First, we consider the merger between two DM halos, with the more massive halo referred to as the “host” and the less massive as the “satellite” halo. The Press-Schechter formalism and our merger tree consider as “merged” two halos that become closely gravitationally bound to each other. However, if the mass ratio of a halo pair is large, then in reality the smaller halo can end up as a satellite halo, and its central BH will never merge with that of the more massive halo. We therefore require in our models that for BHs in such halo pairs to coalesce, the halo merger timescale must be shorter than the Hubble time. We take the standard parametrization of the merger time:

$$\tau_{\text{merge}} \approx x \frac{M_1}{M_2} \tau_{\text{dyn}} \approx 0.1x \frac{M_1}{M_2} t_{\text{Hub}},$$

where  $M_1/M_2 > 1$  is the ratio of the halo masses,  $x \lesssim 1$  is some dimensionless factor that encodes the orbit geometry (e.g. circularity) and dynamical friction, and  $\tau_{\text{dyn}}$  and  $t_{\text{Hub}}$  are the dynamical and Hubble times, respectively. It has been suggested (Boylan-Kolchin et al. 2006) that radial infall along filaments may be preferred in the mergers of elliptical galaxies. Boylan-Kolchin et al. (2008) give a fitting formula for the merger time based on numerical simulations. Their Equation (5) reduces approximately to  $\tau_{\text{merger}}/\tau_{\text{dyn}} \approx 0.45$  for a moderately non-circular orbit with circularity (defined as the ratio of the orbit’s specific

angular momentum to the angular momentum of the circular orbit with the same energy) of 0.5. We take a moderate value of  $x \approx 0.5$ . That is, if  $M_1/M_2 < 20$ , then the BH in the smaller halo is considered to be “stuck” out in the orbiting satellite halo and never merges with the central BH of the more massive halo. This choice also ensures that the vast majority of BH binaries in our simulation do not have extreme mass ratios, as the BH masses co-evolve with the host halos.

We next make assumptions regarding the timescales involving BH dynamics in their host halos, as follows: (1) if the two merging halos each contain a central BH, the two holes are assumed to form a binary efficiently, i.e. we assume there is no delay, in addition to the time taken by the DM halos to complete their merger; (2) the binary is then assumed to coalesce in a timely fashion, prior to the interaction with a third hole; and (3) the binary coalescence is assumed to take place at the center of the potential of the newly merged halo. The first assumption has been addressed by Mayer et al. (2007), who report that the increased drag force of gas in wet mergers allows the timely formation of supermassive BH binaries. The second assumption is valid for binaries in extremely gas-rich environments (see Milosavljevic & Merritt 2003 for a review), or in triaxial galaxies (Berczik et al. 2006). As for the third assumption: given that the timescales of orbital damping are comparable to the intra-merger timescale for BH velocities of  $\gtrsim \sigma_{\text{SIS}}$ , unperturbed BHs free-falling during the halo merger process are likely to end up near the center of the potential within the merging timescales of their hosts. We do not include triple-BH interactions in our analysis.

The assumption that BH binaries merge efficiently following the mergers of their host halos may be unjustified in our models in which initially, the DM halo is devoid of gas, since gas is generally believed to be necessary for prompt coalescence. However, this inconsistency will not affect our conclusions, for the following reasons. First, we find that a BH merger in a gasless environment is a rare event, as it occurs only if both parent halos are low-mass halos that had formed seed BHs relatively recently (i.e. neither halos have yet grown in mass by a factor of 10). Second, members of such binaries will have equal (or, in actuality, similar) masses, since they have not been able to add to their seed mass by accretion. If the BHs can merge efficiently without gas, the coalesced product will likely be ejected, owing to a shallow halo potential and a relatively large kick of an equal-mass merger. If the binary does not coalesce efficiently, it will coalesce once the parent halo merges with a gas-rich, BH-free halo, or once the parent halo accretes enough gas to facilitate the merger. Such belated mergers will also presumably take place with a mass ratio of close to unity and will likely result in ejection, regardless of whether significant gas accretion takes place before coalescence. Now, consider the case of a stalled binary encountering a third BH before gas enrichment of the halo. If the third BH is much more massive, it will not be ejected by gravitational interaction or recoil. There will be a massive BH in the center of the host

halo, and whether the two smaller seed BHs were ejected or swallowed by the larger BH is of little consequence to our analysis, especially given the rarity of double-seed binaries. Thus, inefficient binary coalescence is of concern only when a double-seed binary encounters a third BH of comparable mass before the host halo is gas-enriched. Such triple-seed systems are likely to be extremely rare indeed, and unlikely to affect the overall mass function at  $z = 6$ . We anticipate that the main effects of a gas-depleted host halo will be increasing the number of similar-mass mergers following the initial epoch of seed formation, and slightly reducing the time available for gas accretion.

## 2.5. Gravitational Recoil

### 2.5.1. Probability Distribution of Kick Velocities

To calculate the recoil velocities of coalesced BHs, we employ the formulae provided in Baker et al. (2008), which are used to fit their numerical results,

$$v_{\text{recoil}}^2 = v_m^2 + v_{\perp}^2 + v_{\parallel}^2 + 2v_{\perp} (v_m \cos \xi + v_{\parallel} \sin \xi), \quad (5)$$

$$v_m = A\eta^2 \sqrt{1 - 4\eta} (1 + B\eta), \quad (6)$$

$$v_{a\parallel} = H \frac{\eta^2}{1+q} (a_1 \cos \theta_1 - qa_2 \cos \theta_2), \quad (7)$$

$$v_{a\perp} = -K \frac{\eta^3}{1+q} [a_1 \sin \theta_1 \cos(\phi_1 - \Phi_1) - qa_2 \sin \theta_2 \cos(\phi_2 - \Phi_2)], \quad (8)$$

where  $q \equiv m_2/m_1 \leq 1$  is the binary mass ratio,  $\eta \equiv q/(1+q)^2$  is the symmetric mass ratio, and  $\theta_{1,2}$  are the angles between the BH spin vectors  $\vec{a}_{1,2} = \vec{S}_{1,2}/m_{1,2}$  and the binary orbital angular momentum vector. The angles  $\phi_{1,2}$  denote the projection of the spin vectors onto the orbital plane, measured with respect to a fixed reference angle. As seen from the equations themselves,  $v_m$  is the kick component that depends only on the symmetric mass ratio;  $v_{a\parallel}$  and  $v_{a\perp}$  depend on the mass ratio and the projection of the binary spins parallel and perpendicular, respectively, to the orbital angular momentum. <sup>3</sup>  $\Phi_1(q) = \Phi_2(1/q)$  are constants for a given value of  $q$  that encode the dependence of the kick and orbital precession on the initial spin configuration. We use the mean values given in Baker et al. (2008) for the fitting parameters:  $A = 1.35 \times 10^4 \text{ km s}^{-1}$ ,  $B = -1.48$ ,  $H = 7540 \text{ km s}^{-1}$ ,  $K = 2.4 \times 10^5 \text{ km s}^{-1}$ , and  $\xi = 215^\circ$ . We assume spherical symmetry in our host DM halos, so we are concerned only with the recoil magnitudes and not with the kick orientations.

---

<sup>3</sup>Note that this notation differs slightly from Baker et al. (2008) – we have simplified their notation to be more transparent in our spherically symmetric geometry.

Following Schnittman & Buonanno (2007), for every recoil event, we assign to both members of the binary spin magnitudes in the range  $0.0 \leq a_{1,2} \leq 0.9$ , randomly selected from a uniform distribution. We consider two scenarios for the spin orientation: a case where the orientation is completely random, with  $0 \leq \theta_{1,2} \leq \pi$  and  $0 \leq \phi_{1,2} \leq 2\pi$  chosen randomly from a uniform distribution; and one where the spins are completely aligned with the orbital angular momentum vector.<sup>4</sup> The latter scenario is motivated by Bogdanovic et al. (2007), who argued that external torques (such as those provided by a circumbinary accretion flow) may help align the binary spins with the orbital angular momentum prior to coalescence, making kicks of  $\gtrsim 200 \text{ km s}^{-1}$  physically unfavored. While the argument was originally used to explain the lack of quasars recoiling along the line of sight at lower redshifts (Bonning et al. 2007; although see Komossa et al. 2008 for a candidate recoil detection), the same spin–orbit alignment will also impact the early assembly history of SMBHs, by allowing less massive halos to retain recoiling BHs.

Berti & Volonteri (2008) have provided a merger–tree model to follow the spin evolution of BHs through gas accretion and binary merger events. In this work, we opt not to track the spins of individual BHs due to the uncertainties involved. For instance, if circumbinary disks can act to align the spins of each binary member, this would present a scenario significantly different from the scenario presented by Berti & Volonteri. As we will show in later sections, the spin prescription does not appear to play a primary role in determining the mass function of  $z = 6$  BHs.

We show the recoil velocity distribution for both orientation scenarios as a function of the mass ratio  $q$  in Figure 2. The figure shows the mean,  $1\text{-}\sigma$ , and maximum values for the recoil velocity magnitude from  $10^6$  random realizations at a given value of  $0.01 \leq q \leq 1$ . For  $q > 0.1$ , if spins are randomly oriented then kicks for similar-mass mergers are in the  $100 - 1000 \text{ km s}^{-1}$  range, with a handful of kicks above  $1000 \text{ km s}^{-1}$  and a maximum possible kick of  $\approx 3000 \text{ km s}^{-1}$ ; for spins aligned with the orbital angular momentum, kicks are typically below  $200 \text{ km s}^{-1}$ , with the maximum allowed kick no more than  $300 \text{ km s}^{-1}$ . For  $q \gtrsim 0.1$  and for random spin orientations, the maximum kick  $v_{\text{max}}(q)$  is achieved close to where  $v_{\parallel} \gg v_{\perp}$  is maximized; this occurs when  $a_{1,2} = 0.9$ ,  $\cos(\phi_{1,2} - \Phi_{1,2}) = 1$ , and  $\sin \theta_1 \approx -\sin \theta_2 \approx 1$ . At these spin parameter values,  $v_{\text{max}}(q)$  is well approximated by  $\sqrt{v_m^2 + v_{\parallel}^2}$ , and is a monotonically increasing function of  $q$ . If the spins are aligned with the orbital angular momentum vector, then  $v_{\parallel} = 0$  and the maximum kick occurs when  $a_1 = 0.0$ ,

---

<sup>4</sup>Both cases have the computational advantage that one does not require the values for  $\Phi_{1,2}(q)$ . For a totally random spin orientation and a given value of  $q$ , choosing  $\phi_{1,2}$  randomly is equivalent to choosing  $\phi_{1,2} - \Phi_{1,2}$  randomly. When the spins are aligned with the orbital angular momentum,  $\Phi_{1,2}$  terms are irrelevant because they are always multiplied by  $\sin \theta_{1,2} = 0$ .

$a_2 = 0.9$ . Also, in this aligned case, the spin-independent component  $v_m$  is the dominant term for  $q \lesssim 0.6$  and peaks at  $q \approx 0.345$ , resulting in the maximum and mean values for the recoil speed peaking between these  $q$  values.

### 2.5.2. Trajectories of Kicked Black Holes

Given the mass distribution of the host halo and a recoil speed generated from the method detailed in the previous subsection, we numerically integrate the equation for the radial motion of a BH with mass  $m$ ,

$$\frac{dv}{dt} = -\frac{GM(r)}{r^2} + a_{\text{DF}} - v\frac{\dot{m}}{m}, \quad (9)$$

where  $r(t)$  is the radial displacement of the BH from the center of the host halo and  $v(t)$  is the BH's radial velocity. The first term on the right-hand side is the acceleration due to Newtonian gravity with  $M(r)$  the total (dark matter + baryon) mass enclosed inside spherical radius  $r$ ; the second is the drag deceleration due to dynamical friction; and the third is the deceleration due to mass accretion. A similar calculation of the kicked BH's trajectory has been performed by Madau & Quataert (2004) – the main difference from our prescription is that they assumed the halo to have a collisionless SIS profile, and adopted parameters describing galactic bulges in the local Universe, whereas we use the hybrid DM+gas profile described above, and adopt parameters relevant to low-mass halos at high redshifts.

For a non-collisional medium (in our case, for dark matter), the dynamical friction is described by the standard Chandrasekhar formula (see e.g. Binney & Tremaine 1988),

$$a_{\text{DF}}^{\text{star}}(r, v) = -4\pi G^2 m \rho(r) \frac{1}{v} \ln \Lambda \left[ \text{erf}(X) - \frac{2}{\sqrt{\pi}} X \exp(-X^2) \right], \quad (10)$$

where  $\ln \Lambda$  is the Coulomb logarithm and  $X = v/(\sqrt{2}\sigma_{\text{DM}})$ , with  $\sigma_{\text{DM}}$  the velocity dispersion of the DM halo. In a collisional medium, the density wave in the wake of an object traveling at near or above the sound speed is enhanced via resonance, an effect that has no counterpart in collisionless media. This results in an enhancement of the dynamical friction force, for which Ostriker (1999) has derived an analytical formula. However, the Ostriker prescription is known to overpredict the drag force at slightly supersonic velocities when compared with numerical simulations. While Escala et al. (2004) provides a fitting formula that better fits the numerical results at low speeds, their formula suffers from the opposite problem, and overpredicts the drag for highly supersonic motion. We therefore adopt a hybrid prescription, adopting the Escala et al. (2004) formula for motion with  $\mathcal{M} < \mathcal{M}_{eq}$  and the Ostriker formula

for  $\mathcal{M} > \mathcal{M}_{eq}$ , where  $\mathcal{M}_{eq}$  is the Mach number ( $= |v|/c_s$ ) where the two prescriptions predict equal drag. The entire prescription is described by

$$a_{\text{DF}}^{\text{gas}}(r, v) = -4\pi G^2 m \rho(r) \frac{1}{v} \times f(\mathcal{M}), \quad \text{where :} \quad (11)$$

$$f(\mathcal{M}) = \begin{cases} 0.5 \ln \Lambda \left[ \text{erf} \left( \frac{\mathcal{M}}{\sqrt{2}} \right) - \sqrt{\frac{2}{\pi}} \mathcal{M} \exp(-\mathcal{M}^2/2) \right] & \text{if } 0 \leq \mathcal{M} \leq 0.8; \\ 1.5 \ln \Lambda \left[ \text{erf} \left( \frac{\mathcal{M}}{\sqrt{2}} \right) - \sqrt{\frac{2}{\pi}} \mathcal{M} \exp(-\mathcal{M}^2/2) \right] & \text{if } 0.8 < \mathcal{M} \leq \mathcal{M}_{eq}; \\ \frac{1}{2} \ln \left( \frac{\mathcal{M}+1}{\mathcal{M}-1} \right) - \ln \Lambda & \text{if } \mathcal{M} > \mathcal{M}_{eq}. \end{cases} \quad (12)$$

The Coulomb logarithm  $\ln \Lambda$  is not a precisely known parameter, but is generally agreed to be  $\gtrsim 1$  for both the stellar and the gaseous cases. We adopt the value  $\ln \Lambda = 3.1$  used in Escala et al. (2004), which yields  $\mathcal{M}_{eq} \approx 1.5$ .

The drag force depends on the local gas sound speed. Instead of attempting to compute a temperature profile explicitly, we make the approximation that the gas sound speed is constant and given by the isothermal sound speed of the halo virial temperature. We believe this to be justified from numerical simulation results that show the gas temperature to vary by at most a factor of  $\approx 3$  within the virial radius despite a steeper-than-isothermal ( $\propto r^{-2.2}$ ) density profile (see, e.g. Machacek et al. 2001). While local variations in the sound speed may have significant effects when  $v \sim c_s$ , the recoil events of interest here are for the most part highly supersonic. Recoil events with  $v \sim c_s$  will result in quick damping of the BH orbit and for the purposes of this paper will in all likelihood be indistinguishable from the zero-recoil calculation in terms of their accretion history.

The virial temperature is given by (e.g. Barkana & Loeb 2001)

$$T_{\text{vir}} \approx 370(1+z) \left( \frac{\mu}{0.6} \right) \left( \frac{M}{10^7 M_{\odot}} \right)^{2/3} \left( \frac{\Omega_0 h^2}{0.14} \right)^{1/3} \text{ K}, \quad (13)$$

and the isothermal sound speed is

$$c_s \approx 1.8 (1+z)^{1/2} \left( \frac{M}{10^7 M_{\odot}} \right)^{1/3} \left( \frac{\Omega_0 h^2}{0.14} \right)^{1/6} \text{ km s}^{-1} \quad (14)$$

We also employ a simplified prescription for the velocity dispersion of non-collisional matter, given by the SIS expression evaluated at the virial radius:  $\sigma_{\text{SIS}} = \sqrt{GM/2r_{200}}$ . The simplified expression agrees with the exact velocity dispersion for the NFW profile within  $\sim 20\%$  inside the virial radius.

Because matter that is bound to the BH does not contribute to dynamical friction, we follow Madau & Quataert (2004) and truncate the density profiles at the BH radius of

influence,  $r_{\text{BH}} \approx Gm/\sigma_{\text{SIS}}^2$ . The density is furthermore assumed to be constant inside this radius. Although the BH will drag with it the surrounding gravitationally bound matter, effectively increasing its mass, the additional mass is small owing to the large initial recoil velocity (e.g. Lippai, Frei & Haiman 2008), and we have ignored this mass-enhancement here.

Figure 3 illustrates the effect of the halo matter distribution on the BH orbit. For each of the three orbits shown in the Figure, we adopt  $M = 10^8 M_\odot$ ,  $m = 10^5 M_\odot$ ,  $z = 20$  and  $v_{\text{kick}} = 100 \text{ km s}^{-1}$ . The black curve shows, for reference, the radial orbit for a pure NFW profile. The red curve corresponds to the case which includes an NFW DM component and a power-law gas profile with  $\rho \propto r^{-2.2}$ . The blue curve is for a halo with an NFW DM component and a TIS gas profile.

In our calculations, we are mainly interested in whether the kicked BH is ejected and lost (i.e., can not contribute to the final SMBH mass at  $z = 6$ ), or is retained (i.e., eventually returns to the nucleus, and can be incorporated into the  $z = 6$  SMBH). We place the following retention condition for recoiling BHs: the BH must return to within 1/10th of the virial radius of the newly merged host halo within 1/10th of the Hubble time. The fate of a (SM)BH placed in an orbit extending to the outskirts of its host halo is uncertain: even if it is not lost through tidal interactions with an incoming merging halo, it is not likely to form a binary that hardens efficiently. We therefore impose the above conservative cutoff, in order to avoid tracking these vagrant BHs. Our retention threshold velocity,  $v_{\text{ret}}$ , above which recoiling BHs do not return within the prescribed time limit and are considered lost, is a numerically calculable function of  $M$ ,  $m$ ,  $z$  and halo composition. In order to minimize computation time, we tabulate  $v_{\text{ret}}$  in the range  $5 < z < 40$ ,  $10^5 M_\odot < M < 10^{15} M_\odot$  and  $10^{-6} < m/M < 1$  and approximate the result with a fitting formula that accurately reproduces the exact numerical results within 5% in the tabulated range. In principle, we should compute the retention velocity as a function of the time to the next merger experienced by the halo. However, we find the time dependence to be weak. The distribution of the time intervals between halo mergers in a given merger tree has a sharp peak at  $\approx 10^{-1} t_{\text{Hub}}$ , with far fewer mergers occurring at  $\sim 10^{-2} t_{\text{Hub}}$  and  $\sim t_{\text{Hub}}$ . At these tails of the distribution,  $v_{\text{ret}}$  varies by  $\lesssim 10\%$  from the value for  $10^{-1} t_{\text{Hub}}$ . We find that  $v_{\text{ret}} \sim 5 - 8 \times \sigma_{\text{SIS}}$ . This is comparable to the escape velocity for a *non-dissipative* pure SIS profile that is truncated at the BH radius of influence,  $v_{\text{esc}} \approx 5\sigma_{\text{SIS}}$  if  $m = 10^{-3} M$  (YM04).

The weak dependence on  $v_{\text{ret}}$  on the return time limit is a counterintuitive result, but it can be understood as follows. There is a minimum kick speed that is required to displace the hole beyond  $0.1r_{200}$ , which represents  $\lim_{t \rightarrow 0} v_{\text{ret}}$ ; and there is a maximum kick,  $\lim_{t \rightarrow \infty} v_{\text{ret}}$ , beyond which the BH remains completely unbound from the halo, even in the presence of



drag.  $v_{\text{ret}}(t)$ , then is a function of time that is always between these two extreme values. However, owing to the high central density of our gas-dominated halos, the difference between these two limits is small,  $\sim 10\%$ . Since this difference is smaller than other model uncertainties, such as those stemming from discrepancies from the actual density profile of high-redshift DM halos (e.g. clumping or triaxiality) and the merger tree prescription, we simply use the retention velocity computed for the approximate median time limit,  $0.1t_{\text{Hub}}$ .

Finally, for simplicity, we treat the halo as a static mass distribution during each recoil event. That is, we ignore the cosmological evolution of the DM potential, and we assume that the recoiling BH does not affect the medium by clumping or heating it. Note, however that the latter feedback may play a nontrivial role in real systems, since the kinetic energy of a recoiling hole can be comparable to the gravitational binding energy of the entire host halo and can be expected to cause significant disruption of the surrounding matter.

## 2.6. The Black Hole Accretion Rate

We turn now to our prescription for the accretion rate of the BHs in our model. Of particular interest is the possibility that the gravitational recoil effect will significantly limit the ability of kicked BHs to accrete gas, by displacing them into low-density regions for prolonged periods, and/or by limiting through high relative velocities the amount of gas that can be gravitationally captured. One can imagine a scenario in which a SMBH whose progenitors have survived numerous kicks but have spent long episodes in underdense regions may have a final mass much less than that predicted by simple Eddington growth. We therefore follow the accretion rate self-consistently, as the recoiling holes proceed along their radial orbits. Specifically, in our models a BH embedded in gas is assumed to undergo standard Bondi-Hoyle-Littleton (BHL) accretion,

$$\dot{m}(r, v) = \frac{4\pi G^2 \rho_b(r)}{(c_s^2 + v^2)^{3/2}} m^2. \quad (15)$$

The accretion rate is capped at the Eddington rate,

$$\dot{m} = \frac{1 - \epsilon}{\epsilon} \frac{m}{t_{\text{Edd}}}, \quad (16)$$

where  $t_{\text{Edd}} = 44\text{Myr}$  and  $\epsilon$  is the radiative efficiency, for which we assume  $\epsilon = 0.10$ .

If the gas density is too low, or if the sound speed or its velocity with respect to the disk too high, a BH may not be able to accrete at the Eddington rate even if it is close to the center of a halo. Because the BHL rate is proportional to  $m^2$ , an underfed BH with initial

mass  $m_0$  will eventually reach the Eddington accretion rate ( $\propto m$ ) at a threshold mass

$$m_{\text{Edd}} = \frac{1 - \epsilon}{\epsilon} \frac{c_s^3}{4\pi G^2 \rho_b t_{\text{Edd}}} \approx 3500 \left( \frac{c_s}{4 \text{ km s}^{-1}} \right)^3 \left( \frac{\rho_b}{M_\odot \text{pc}^{-3}} \right)^{-1} M_\odot, \quad (17)$$

where  $4 \text{ km s}^{-1}$  is the isothermal sound speed for an ionized hydrogen gas at 1200K. The typical central density of a 1200K halo with a TIS gas profile is  $\sim 5 \times 10^{-3} (1+z)^{7/3} M_\odot \text{pc}^{-3}$ . Sub-Eddington accretion rates are not an issue for BHs in a power-law gas profile, as the steep profile provides a sufficient central density for immediate Eddington accretion.

The time it takes for a BH with  $m_0 < m_{\text{Edd}}$  to reach this threshold mass, assuming that the local density remains constant, is

$$t_{\text{crit}} = \left( \frac{m_{\text{Edd}}}{m} - 1 \right) \frac{\epsilon}{1 - \epsilon} t_{\text{Edd}} \approx 2.7 \left( \frac{m_0}{100 M_\odot} \right)^{-1} \left( \frac{c_s}{4 \text{ km s}^{-1}} \right)^3 \left( \frac{\rho_b}{M_\odot \text{pc}^{-3}} \right)^{-1} \text{Gyr}. \quad (18)$$

$t_{\text{crit}} \sim$  a few 100 Myr for  $100 M_\odot$  halos embedded in 1200K TIS halos at  $z \gtrsim 20$ , and  $t_{\text{crit}} \gtrsim$  Gyr for  $z \lesssim 14$ . This means that for TIS gas profiles, seed holes will spend a significant fraction or all of the available time prior to  $z \approx 6$  accreting below the Eddington rate.

The difference between BHL and Eddington accretion rates as they relate to BH growth is also discussed in Volonteri & Rees (2006). However, in that paper the context is for the direct formation of  $m > 10^4 M_\odot$  intermediate-mass BHs through super-Eddington BHL accretion. We here adopt the opposite extreme assumption, i.e. that the BH radiates efficiently at all times, and its accretion rate obeys the Eddington limit. The BHL rate can then initially be sub-Eddington in TIS halos, owing to the low BH mass and low gas density (the baryon density required to fuel BHL accretion at the Eddington rate was also discussed by Turner 1991).

To illustrate the impact of extended sub-Eddington growth phases, we perform a simple analytical calculation. Suppose that a BH is formed with mass  $m_{\text{seed}}$  at redshift  $z$  in a halo with virial temperature 1200K, and that the local gas density is held constant at the value when the BH was formed. Note that for this exercise, we assume that gas density is constant even as the halo around the BH is growing by merging with other halos – in other words, we assume these mergers deliver gas to the nucleus containing the original BH, roughly maintaining a constant density at the Bondi radius around the BH. Figure 4 shows the maximum possible mass that can be attained by such a BH growing in isolation through gas accretion alone, assuming that the accretion rate is determined solely by Equations (15) and (16) and that accretion is not supply-limited. If the host halo has a steep power-law cusp, the accretion rate is Eddington throughout regardless of when the seed BH is formed.

However, if the central fuel density is low, then it is possible for the local BHL accretion rate to be significantly sub-Eddington initially. In such a scenario, the earliest forming seeds are the only ones able to reach the Eddington rate; the late-forming seeds are unable to reach the Eddington rate before  $z = 6$ . In this scenario the late-forming seeds, which are easily identifiable by the drastically shallower growth slope in the figure, cannot grow rapidly enough to contribute to the SMBH population. Note that assuming a constant gas density in this calculation gives an optimistic accretion rate for the TIS case, as in those profiles the central gas density generally decreases with Hubble expansion and significantly reduce the BHL rate.

It is computationally expensive to numerically integrate the individual orbits and accretion histories of every recoiling BH in our simulations. We therefore tabulate the accretion growth in Eddington units during the first  $0.1t_{\text{Hub}}$  of the orbit, and describe the results in a fitting formula in the same manner as we have done for the retention velocity. Given a specific prescription for the baryon distribution, we tabulate across four relevant variables in the following ranges:  $10^5 M_\odot < M < 10^{15} M_\odot$ ,  $10^{-6} < m/M < 1$ ,  $5 < z < 40$ , and  $0 < v_{\text{kick}}/v_{\text{ret}} < 1$ .

In the absence of a kick, and if the accretion rate were always at the Eddington limit, the SMBH mass in a given halo at  $z \approx 6$  is easily approximated by

$$m_{\text{SMBH}} \approx N_{\text{seed}} \exp\left(f_{\text{duty}} \frac{\epsilon}{1 - \epsilon} \frac{t_{\text{seed},6}}{t_{\text{Edd}}}\right) m_{\text{seed}}, \quad (19)$$

where  $m_{\text{seed}}$  is the seed BH mass,  $N_{\text{seed}}$  is the number of seeds in the merger history of the halo,  $t_{\text{seed},6}$  is the available time between the typical seed formation time and  $z \approx 6$  and  $f_{\text{duty}}$  is the time-averaged duty cycle for accretion. Equation (19) represents the ideal, maximally efficient scenario for SMBH assembly, and we can use it to effectively measure the cumulative impact of underfed accretion, recoil-induced ejection, and other factors that limit the assembly efficiency.

The measurements of clustering of quasars in the SDSS suggest that the duty cycle of active (luminous) accretion increases steeply with redshift at  $3 \lesssim z \lesssim 6$ , with the most active quasar BHs at  $z \approx 6$  showing  $0.6 \lesssim f_{\text{duty}} \lesssim 0.9$  (Shen et al. 2007; Shankar et al. 2008). We therefore adopt duty cycles of  $\geq 0.6$ . Although it is likely that SMBHs regulate their own growth through feedback mechanisms, we do not address such scenarios a priori. To keep our models as simple as possible, we will only impose the loosest upper limit on the SMBH accretion rate: they must not accrete more mass than there the total mass of baryons in the host halo. However, we will discuss an alternative ad-hoc model below, which is able to reproduce the well-known relation between SMBHs and the velocity dispersions of the bulges of host galaxies (the  $m$ - $\sigma$  relation).

## 2.7. Putting Together the $z = 6$ SMBH Mass Function

Explicitly constructing the SMBH mass function at  $z = 6$  over a wide mass range is computationally intractable. The host halo mass inferred from the observed quasar space density from the  $z \sim 6$  quasars is several  $\times 10^{12} M_\odot$  (e.g. Fan 2006). For every halo with this mass, there are  $\sim 10^7$  halos with  $10^8 - 10^9 M_\odot$ . Blindly calculating the SMBH mass for every halo with  $M > 10^8 M_\odot$  using our trees-plus-orbits algorithm would be prohibitively expensive computationally.

We therefore carry out a piecewise calculation of the SMBH mass function that is computationally tractable. The procedure is as follows: (1) We group the halo population into logarithmic mass bins of size  $x < \log_{10} M < x + \Delta x$ ; (2) For each bin, we select  $\gtrsim 10^2 - 10^4$  individual Monte-Carlo-generated halos with masses randomly generated from the Press-Schechter distribution at  $z = 6$ ; (3) We simulate the BH population for each such halo using our trees-plus-orbits algorithm, and assume the resulting sample is representative of all  $z = 6$  halos in the mass bin; (4) For each bin we multiply the sample by the appropriate weight to construct the entire Press-Schechter halo mass function,  $\int_x^{x+\Delta x} dN/d \ln M d \ln M$ ; and finally (5) Sum the contributions from each bin. The result is a Press-Schechter distribution of halos with  $M > 10^8 M_\odot$  at  $z = 6$ , with a statistical representation of the corresponding SMBH mass function. The bins used and their relevant properties, including the number of Monte-Carlo halos that were cloned to populate the full mass function, are listed in Table 1. This numerical shortcut is not used for the most massive halos. 40 halos are expected above  $10^{12.85} M_\odot$ , and these are simulated individually.

This method allows a fast calculation of the BH mass function, with the caveat that there must be enough BHs in each bin to keep statistical uncertainties to a minimum. Unfortunately, this is not always preventable for models with extremely low  $f_{\text{seed}}$ , and the reader will notice statistical noise in the results of such models. In some cases, we increase the halo sample by a factor of 10 in an attempt to reduce the errors.

In all, our simulations represent the Press-Schechter population of DM halos in a comoving volume of  $\approx 280 \text{Gpc}^3$ , roughly equal to the comoving volume that was probed by the SDSS between  $z \approx 5.7 - 6.4$ . We have simulated a total of  $\approx 1.17 \times 10^5$  DM halos (see the column  $N_{\text{sim}}$  in Table 1), and through the procedure described above extrapolated the results to represent the  $\approx 3 \times 10^{12}$  Press-Schechter halos (with  $M > 10^8 M_\odot$ ) expected to be present in the  $280 \text{Gpc}^3$  volume.

### 3. Results and Discussion

#### 3.1. Building the $> 10^9 M_\odot$ SMBHs

As stated in the Introduction, our primary goals are (i) to understand the possible ways in which the  $> 10^9 M_\odot$  SMBHs may have been assembled at redshift  $z > 6$ , and (ii) whether the *LISA* event rates are sufficiently different in competing models so that one can disentangle the physical assembly scenario from the *LISA* data stream. As a first step toward these goals, we would like to survey all feasible combinations of the physical assembly parameters, understand the impact of each model parameter, and look for corresponding give-away features in the predicted *LISA* stream.

Although a broad simulation survey is beyond the scope of this paper, we have undertaken a cursory tour of the basic parameter space. We begin by considering two basic seed models:  $100 M_\odot$  seeds forming as remnants of Pop III stars in minihalos when they first reach the virial temperature  $T_{\text{vir}} \geq T_{\text{seed}} = 1200\text{K}$  and  $10^5 M_\odot$  seeds forming as a result of direct collapse of gas in halos when they first reach  $T_{\text{vir}} \geq 1.5 \times 10^4\text{K}$ . For each case, we consider halos with an NFW DM component and a gaseous component with either a cuspy  $\rho_{\text{gas}} \propto r^{-2.2}$  power-law or a corey TIS profile. The TIS models consistently failed to produce SMBHs by  $z = 6$ , with typical maximum BH masses of  $\lesssim 10^3 M_\odot$ . In those models the central gas densities are too low to allow for prolonged episodes of accretion near the Eddington rate, as noted in Section 2.5 above.

For each type of seed, we vary three sets of parameters: (i) the seeding fraction  $10^{-3} \leq f_{\text{seed}} \leq 1$ , i.e. the probability that a halo reaching the critical temperature will form a seed BH; (ii) the time-averaged accretion rate in Eddington units, characterized by the duty cycle  $f_{\text{duty}}$ , for which we use  $f_{\text{duty}} = 0.6, 0.8$  and  $1.0$  (note that  $f_{\text{duty}}$  and the radiative efficiency  $\epsilon$  are degenerate in our prescription; see below); and (iii) whether at the time of their merger, the BH spins are randomly oriented or aligned with the orbital angular momentum of the binary. The spin magnitudes are chosen from a uniform random distribution  $0 < a_{1,2} < 0.9$  (Schnittman & Buonanno 2007). We do not track the evolution of BH spins in our models. While more rapidly spinning BHs are capable of accreting at higher efficiency, we neglect this effect and assume a global efficiency coefficient in our models. Of the four main ingredients of the SMBH assembly introduced in § 1 above, we here therefore vary three: the seed rarity, the accretion rate, and the recoil dynamics. For the fourth, the merger rate, we have simply assumed that BHs merge when their parent halos do, as extreme-mass BH binaries are rare in our simulation, given the threshold we have imposed on the mass ratio for halo mergers. We will call the above our fiducial set of parameters.

For each realization, we compute the mass function of BHs at  $z = 6$  with  $m > 10^5 M_\odot$ ;

the rate of events in the *LISA* observational mass range,  $\sim 10^{4-7}/(1+z)M_\odot$ ; the fraction of DM halos hosting a central massive BH; and  $m/M$ , the ratio between the mass of the SMBH and its host DM halo, which serves as a proxy for the  $m$ - $\sigma$  relation.

We begin with Figure 5, showing the mass function for the  $m_{\text{seed}} = 100M_\odot$  Pop III seed model. This and the companion figures are organized with different values for  $f_{\text{seed}}$  in different columns, the two spin prescriptions in different rows, and the different duty cycles in different line styles (and different colors, in the online version). This will be the default organization of our 8-panel figures unless noted otherwise.

The numbers in the upper-right-hand corner of each panel represents the total SMBH mass density,  $\log_{10}[\rho_\bullet/(M_\odot \text{ Mpc}^{-3})]$ , for all BHs with  $m > 10^5 M_\odot$ . Because of statistical fluctuations, for multiple model realizations with identical parameters this value can vary by  $\lesssim 10\%$  for  $f_{\text{seed}} \gtrsim 10^{-1}$ , and as much by a factor of a few for  $f_{\text{seed}} \lesssim 10^{-3}$ . For each of these simple models, this density is exceedingly high compared to the SMBH density of the local universe. For the present discussion, we will overlook this point as we address the effects of the various model factors; we will introduce the additional constraint from  $\rho_\bullet$  in subsequent sections.

The most stringent observational requirement for the high-mass end of the  $z \approx 6$  SMBH mass function comes from the SDSS observation of the  $z \approx 6.4$  quasar J1054+1024, which has an inferred mass of  $\sim 4 \times 10^9 M_\odot$ . Since this object was detected in a region  $\sim 10\%$  of the sky, we estimate that  $\gtrsim 10$  similar objects may exist at  $z \sim 6$ . We have adopted this as a rough indication of the lower limit of the SMBH mass function at redshift  $z = 6$ , and represent this limit by the upper right quadrangle in each of the panels, delineated by the red dashed lines. Note that these lower limits are conservative, since they do not require the presence of any additional SMBHs with comparable mass that are “off”. Since high values for the duty cycle – near unity – are suggested by quasar clustering measurements (as discussed above), and are also required for growing the most massive SMBHs (as we find below), this correction is only of order a factor of  $\sim$ two. As seen in the figure, the high-mass end of the SMBH mass function is so steep that increasing the lower limit on the required SMBH space density by even  $\sim 2$  orders of magnitude would make little difference to our conclusions.

The first conclusion one can draw from this figure is that several combinations of parameters can produce SMBHs massive enough to power the quasar J1054+1024. We will return to this and other observational constraints in the next subsection, but let us for now focus on understanding the effects of our various parameters and their combinations. In general, the effect of varying each of the parameters is relatively straightforward to understand. Increasing the accretion rate, increasing the seed occupation fraction, and aligning the spins

all tend to result in more massive BHs. Note that the accretion rate in Eddington units,  $f_{\text{duty}}$ , is degenerate with the accretion efficiency, as  $\dot{m} \propto f_{\text{duty}} \times (1 - \epsilon)/\epsilon$ . For example, a model with  $\epsilon = 0.15$  and  $f_{\text{duty}} = 1.0$  is equivalent to  $\epsilon = 0.10$  and  $f_{\text{duty}} = 0.63$ . We have used  $\epsilon = 0.10$  throughout the results presented here. With this value for the efficiency, it is possible to build the most massive SDSS quasar SMBHs by  $z \approx 6$ , starting with  $100M_{\odot}$  seeds. If the efficiency is  $\approx 0.15$ , however, it is only possible to build the SMBHs in question with the most optimistic assumptions:  $f_{\text{duty}} \approx 1$ ,  $f_{\text{seed}} \gtrsim 0.1$ , and spin alignment would all be required.

We note two non-trivial observations to be made from Figure 5. First, if the seed fraction is low, the spin orientation has a minimal effect on the BH mass function. This is because if seeds are extremely rare, they are likely to grow in isolation for much of their existence along with their host halos. The first mergers are not likely to occur until the gravitational potentials of their host halos are deep enough to retain them from any recoil event. Second, the increase in the SMBH abundance from increasing the seeding fraction has a tendency to plateau. This is the reverse situation compared to the low  $f_{\text{seed}}$  limit: if seeds are very common, they are likely to experience multiple BH mergers very early in the merger tree, when their masses are still comparable, and ejections become very common. As  $f_{\text{seed}}$  increases, assembly becomes increasingly inefficient at early times. In models where the seeding halo temperatures are lower, the efficiency saturates at lower values of  $f_{\text{seed}}$ . Furthermore, in models with the shallower TIS gas profiles, we find that increasing the occupation fraction beyond a certain “sweet spot” value rapidly decreases the final SMBH masses. The reasons for this are that (i) the seed BHs in these models barely grow, making near-equal mass ( $q \sim 1$ ) BH mergers, and therefore large kicks, much more common and (ii) the gas drag is reduced, making it easier to kick holes out of these halos. We conclude that arbitrarily increasing the number of seed holes contributing to the assembly process is not necessarily an efficient solution to the SMBH assembly problem. In fact, excessive seeding can lead to a different conflict with observations – overproducing the mass density in lower-mass SMBHs –, to which we will return in the next subsection.

Let us turn now to Figure 6, which shows the BH occupation fraction in  $M > 10^8 M_{\odot}$  DM halos at  $z = 6$ , and the BH-to-halo mass ratio (which here serves as a proxy for the  $m$ - $\sigma$  relation; see, e.g. Ferrarese 2002) for each of the models. Here, we have arbitrarily defined our occupation fraction to mean the fraction of DM halos that host a BH with a minimum mass of  $10^4 M_{\odot}$ , as we are interested in the population of nuclear BHs and not stellar remnants. Menou et al. (2001) have shown that, in the low-redshift Universe, the fraction of DM halos hosting a SMBH will approach unity, regardless of the initial occupation fraction at earlier times. We find that at  $z \approx 6$ , the occupation fraction in halos with  $M \lesssim 10^{11} M_{\odot}$  can still be significantly below unity, depending primarily on  $f_{\text{seed}}$ . In principle, a future survey that

can determine the quasar luminosity function (LF) at  $z = 6$  to several magnitudes deeper than the SDSS could look for this drop in the occupation fraction, since it will produce a flattening of the LF at magnitudes below some threshold. The spin prescription has a noticeable effect on the  $z = 6$  occupation fraction for  $f_{\text{seed}} \gtrsim 10^{-2}$ . On the other hand, the duty cycle essentially only affects the mass of the BHs, and not their presence or absence, and so has a minimal effect on the occupation fraction, within the parameter range shown. Note that we do not expect to reproduce the  $m$ - $\sigma$  relation in our simulations, as we employ simple and  $z$ -independent accretion and seeding prescriptions, and our models have no feedback to enforce the relation. Instead, the  $m/M$  relation should be taken as a sanity check that we are producing a physically viable BH population. Note that in some of the models shown in Figure 5, the BHs grow much larger than the  $m/M$  relation observed in nearby galaxies. In particular, as the figure reveals, SMBHs in the lower-mass ( $\sim 10^8 M_\odot$ ) halos in the models with  $f_{\text{duty}} = 1$  tend to consume most of the gas in their parent halos, clearly an improbable result.

For an explicit comparison, alongside the  $m/M$  relation produced by our models, we have plotted the value expected based on measurements of the  $m$ - $\sigma$  relation in local galaxies. Specifically, we show the expression from Wyithe & Loeb (2003),

$$m = 10^{12} \epsilon_0 \left( \frac{M}{10^{12} M_\odot} \right)^{\gamma/3} (\Omega_0 h^2)^{\gamma/6} (1+z)^{\gamma/2} \approx 1.16 \times 10^7 \left( \frac{M}{10^{12} M_\odot} \right)^{\gamma/3} (1+z)^{\gamma/2}. \quad (20)$$

We adopt their parameter choices of  $\epsilon_0 = 10^{-5.4}$  and  $\gamma = 5$ . This expression satisfies the SDSS constraints at the high-mass end of the mass function. It also agrees well with the relation suggested by Ferrarese (2002) for SMBHs in the local universe,  $m \sim 10^7 (M/10^{12} M_\odot)^{1.65}$ . As the figure shows, our predicted  $m/M$  relation tends to have the opposite slope than the one inferred from the observed  $m$ - $\sigma$  relation: in our results  $m/M$  decreases with mass or stays roughly constant as  $M$  increases, but this is the opposite of the empirical trend. This is due mainly to the difference in the growth rates of halos and holes: our simple prescription for steady, exponential accretion for the BHs can significantly exceed the growth rate of DM halo masses due to the accretion of unresolved low-mass halos in the EPS merger tree. As a result, in some cases, the host halo mass predicted for the  $z = 6$  quasars is as low as  $10^{11} M_\odot$ , which is an order of magnitude lower than would be predicted from the extrapolation of the locally measured  $m/M$  relation, or from the inferred space density of the host halos (e.g. Haiman & Loeb 2001). However, any extrapolation of the  $m - \sigma$  or  $m/M$  relation to high redshift, and the masses of halos that host the brightest  $z > 6$  quasars, at present, have large uncertainties, and do not robustly preclude such low values. As will be discussed below, the overly rapid growth of SMBHs in this suite of models motivates modifications to the modeling, including a model in which the extrapolated  $m/M$  relation holds by assumption.



Figure 7 shows estimates for the *LISA* event rate, calculated for all binary mergers satisfying  $10^4 M_\odot < (m_1 + m_2)(1 + z) < 10^7 M_\odot$  as (see, e.g. Menou et al. 2001),

$$\frac{d^2 N}{dz dt} = 4\pi c d_{\text{com}}^2(z) \frac{\Delta N}{\Delta z \Delta V}, \quad (21)$$

where  $\Delta N$  is the number of SMBH merger events in the tree in a time step  $\Delta z$  and a simulated comoving volume  $\Delta V$ , and  $d_{\text{com}}$  is the comoving distance. Although there is a mild dependence on the duty cycle / accretion rate and the kick prescription, it is evident that for our assembly models  $f_{\text{seed}}$  has the greatest effect in setting the rate of SMBH binary mergers detectable by *LISA*. Because the initial merger rates scale as  $f_{\text{seed}}^2$ , the measured event rate is extremely sensitive to the BH number population. Since the merger activity peaks near  $z \lesssim 10$ , *LISA* should be able to measure the masses of most of these SMBH binaries to high precision (Hughes 2002, Arun et al. 2008). Although the raw detection rate – without any information on BH spin or mass ratio – alone will be richly informative, the ability to determine the source masses with high fidelity should be very useful in further constraining the growth rate of the first SMBHs, and breaking degeneracies between the allowed parameter-combinations. The observed distribution of binary masses as a function of redshift will provide direct snapshots of the mass function and shed light on its evolution, independently from quasar luminosity surveys (e.g. Yu & Tremaine 2002; Willott et al. 2006).

Another family of assembly models that has been frequently discussed in the literature is the so-called “direct collapse” model, wherein BHs with  $m \sim 10^{4-6} M_\odot$  are formed rapidly from gas cooling via atomic H in halos with virial temperature  $T \gtrsim 10^4 \text{K}$  (Oh & Haiman 2002; Bromm & Loeb 2003; Volonteri & Rees 2005; Begelman et al. 2006; Spaans & Silk 2006; Lodato & Natarajan 2006). We simulate such a family of models, for the same set of the parameters  $f_{\text{seed}}$  and  $f_{\text{duty}}$  and the same spin alignments. We choose  $m_{\text{seed}} = 10^5 M_\odot$  and  $T_{\text{seed}} = 1.5 \times 10^4 \text{K}$ . We show the mass functions, the hole-halo relations and the *LISA* rates (the same information as in Figures 5, 6 and 7) in Figures 8, 9 and 10. Although the main differences are all fairly intuitive, it is instructive to address how the direct-collapse models differ from the Pop-III seed models.

First, from Figure 8 we see that it is much easier to construct more massive SMBHs owing to the larger seed masses. In fact, the models with  $f_{\text{seed}} \gtrsim 0.1$  become unphysical, since the SMBHs in these models would exceed the baryon mass  $(\Omega_b/\Omega_m)M$  of their parent halos. The second point is that the mass function is very differently distributed between the Pop-III and direct-collapse scenarios. The reader will note that for each set of parameters, the overall SMBH density does not differ significantly between the corresponding seed models. However, this is deceiving as the mass function is clearly different, with the direct-collapse seeds resulting in a more “top heavy” SMBH population. For the range of parameters

surveyed, the Pop-III model has  $\gtrsim 90\%$  of the SMBH mass in the  $m < 10^7 M_\odot$  range if  $D = 0.6$ , compared to  $\lesssim 30\%$  for the  $D = 0.6$  direct-collapse seed models. For  $D = 1.0$  and random spin alignment,  $\sim 2 - 5\%$  of the SMBH density resides in the most massive  $m > 10^9 M_\odot$  BHs if the seeds are Pop III; for the same parameters,  $\sim 60 - 70\%$  of the mass is in the billion-plus solar mass BHs in the corresponding direct-collapse models. Note that the total BH mass density remains extremely high; again, we will address this point shortly.

Third, there is a slightly weaker dependence on the spin orientation of the BH binaries. This is most apparent by comparing the  $z = 6$  occupation fractions in Figures 6 and 9, and is due to the deeper potentials of the host halos in the direct collapse case. Fourth, even though the  $m/M$  relation continues to have a slope opposite to the locally observed trend, there appears to be a break in the relation at  $M \sim 10^9 M_\odot$ , accompanied by a drop in the occupation fraction. This is due to the simple fact that halos below this mass threshold cannot have many  $T > 1.5 \times 10^4 \text{K}$  progenitors and the model similarly prohibits intermediate-mass BHs. This cutoff contributes to the top-heaviness of the mass function for these models. Fifth, *LISA* rates are lower by one to two orders of magnitude than in the Pop-III seed models, because there are fewer  $1.5 \times 10^4 \text{K}$  halos than  $1200 \text{K}$  halos (another factor is that the seed BHs are already born with a mass near the middle of *LISA*'s logarithmic mass range, so they spend only  $\sim$  half the time in the *LISA* band, compared to the Pop-III seeds). It is worth noting, in particular, that it is possible to build the SDSS quasar BHs in ways that produce no detectable GW events for observation with *LISA* beyond  $z \sim 6$  (in contrast, in the successful pop-III models, a minimum of a few events are predicted). In such scenarios, SMBHs are extremely rare until  $z \sim 6$ , at which point the SMBH occupation fraction will evolve toward unity fairly rapidly, as described by Menou et al. (2001).

Finally, in Figure 11 we present the mass function and the *LISA* detection rate in five variants of a fiducial  $f_{\text{duty}} = 0.65$ ,  $f_{\text{seed}} = 1$ , aligned spin model with pop-III BH remnant seeds. We choose these values because they just barely are able to match the abundance of the most massive SDSS quasar BHs, and because they produce the most BH mergers, and thus the effects of varying the other recoil-related parameters will be the most discernible. We show the fiducial model in bold. In the modified models, we (i) allow the gas density profile to be shallower, with a  $r^{-2}$  power law – this is to allow for the possibility that the gas surrounding the BH has not cooled and condensed to high density (dark blue curves); (ii) require the BH spins to be near-maximal at  $a_{1,2} = 0.9$ , instead of choosing them randomly from the range 0.0 to 0.9 – this is to allow for the possibility that all SMBHs at high  $z$  are rapidly spinning, e.g. due to coherent accretion (green curves); (iii) allow halos of all mass ratios to merge, where previously we had considered a halo with mass less than 1/20th that of its merger companion to become a satellite (yellow curves); (iv) assume that the Pop III seed progenitors are not able to blow out the gas in the host minihalo (red curves); and (v)

ignore the effects of accretion suppression due to episodes of recoil-induced wandering, and instead assume that all BHs accrete at  $f_{\text{duty}}$  unless ejected (light blue curves).

We also ran models with a TIS profile for the gas component. We found that these models always failed to produce any SMBHs above  $10^6 M_{\odot}$  by redshift  $z = 6$  due to the initial phase of sub-Eddington accretion of seed BHs, and their results are not shown in Figure 11. This implies that SMBHs must be continuously surrounded by dense cores of gas that was able to cool at the centers of DM halos – feeding holes with the low-density gas in DM halos whose gas was unable to cool does not allow for high enough accretion rates (Turner 1991 emphasized the same issue for the growth of  $z \sim 4$  quasar BHs).

The results shown in Figure 11 give insight to the importance of the assumptions that went into our models. In particular, of all the parameters that we have varied for fixed  $f_{\text{seed}}$  and  $f_{\text{duty}}$ , the most significant for the SMBH mass function, by far, are the spin orientation and the limit on the halo mass ratio for timely mergers. Both of these have a similar effect of increasing the number of BHs, especially at the massive end. The former result – that maximizing the spin increases the SMBH mass function – may seem surprising at first, since generally large spins imply larger kicks. However, this is not always the case, as can be understood from equations (5-8). Under the assumption that both spins are aligned with the orbital angular momentum,  $v_{\parallel} = 0$ , and  $v_{\perp} \propto (a_1 - qa_2)$  is maximized for *unequal* spins (i.e.  $a_1 = 1$  and  $a_2 = 0$  for a typical  $q \sim 1$ ); setting  $a_1 = a_2 = 0.9$  therefore eliminates the largest kicks, and allows more BHs to be retained. Comparatively smaller differences are visible in the mass function for the other model variants. Figure 11 also shows that adding in the unequal-mass halo mergers and increasing the spins affect the *LISA* event rates differently: the former adds new events mostly at  $z \lesssim 10$ , where unequal-mass mergers are more common, whereas increasing the spin mostly adds new events at  $z \gtrsim 10$ . Interestingly, ignoring the blow-out has little impact on the SMBH mass function at  $z = 6$ , but it does shift the *LISA* events to higher redshifts, especially at  $z \gtrsim 10$ . Figure 11 suggests that the *LISA* event rate can be useful in disentangling these three effects.

Perhaps the most surprising inconsequential variation is ignoring episodes of reduced accretion due to the BH wandering in low-density outskirts following recoil. The reason for this is simply that lengthy oscillating orbits are relatively rare if the central gas density is high; the BHs either return quickly, or are ejected (by assumption). Recall that our definition for a “retained” BH is that the recoiled hole must return to within 1/10th of the halo’s virial radius within 1/10th of the Hubble time. For low kick speeds, the BH does not get very far, because the gas provides both a steep gravitational potential barrier and a strong dissipative sink. The orbit will thus be rapidly damped, with only very brief periods of underfeeding. If a BH is kicked hard enough to reach the outskirts of the halo, there is very little dissipation

there, to tug it toward the center or to further damp its oscillation. Since the radial velocity at this point is low, it’s likely to remain outside 1/10th of the virial radius for a significant period. The bottom line is that the range of initial kicks that would take the BH to the low-density outskirts to cause significant underfeeding, while still allowing it to return quickly enough to be “retained” is simply negligibly small.

Blecha & Loeb (2008) recently performed a more detailed analysis of the orbits of recoiling SMBHs that include a multi-component halo mass distribution and three-dimensional orbits. They report that recoil velocities of between  $100 \text{ km s}^{-1}$  and the escape velocity lead to significant suppression of the accretion rate, with SMBHs accreting only  $\sim 10\%$  of its initial mass over  $10^6 - 10^9$  years of wandering through the halo. We note that (1) in our simulations we ignore the longest-wandering BHs through our prescribed retention threshold; (2) typical kick magnitudes for SMBHs are lower than  $100 \text{ km s}^{-1}$  in our simulations, a point we explain below; and (3) their prescription of the baryon distribution results in a lower central density than our models, as in that paper they are concerned with typical galaxies at low redshift, and not with minihalos and protogalaxies. We conclude that prolonged periods of wandering and underfeeding are unlikely to have a significant effect on the mass function of high- $z$  SMBHs as a whole. Oscillations may play a more prominent role in the growth history of SMBHs if large kicks are more common (and the retained holes tend to be marginally retained), if the halo gravitational potential is more shallow, or if the effect of dynamical friction on BH orbits is less than what we have considered in this paper. Also, halo triaxiality (Blecha & Loeb 2008) and/or a clumpy mass distribution (Guedes et al. 2008) could increase the time that kicked holes take to return to the halo center (or they may never return). In principle, this may increase the impact of these oscillations. However, in practice, the inner, baryon-dominated regions of the galaxies are likely close to smooth and spherical. The BHs that are not ejected in our models typically do not leave these regions and so will not be subject to large changes in their orbits from these effects.

The results presented thus far seem to paint a relatively simple set of relevant parameters for SMBH assembly. There is the seeding function  $f_{\text{seed}}$ , which governs the BH merger rate and therefore to a large extent the *LISA* event rate. The event rate also depends on the time-averaged accretion rate, parameterized here by the duty cycle  $f_{\text{duty}}$ , and the initial seed mass  $M_{\text{seed}}$ , as these set the evolution of the observable mass spectrum. The seeding prescription and  $f_{\text{duty}}$  determine the mass function almost entirely if  $f_{\text{seed}} \ll 1$ . If  $f_{\text{seed}} \gtrsim 0.1$ , then the spins of the BH binary play a role in setting the recoil speeds and the subsequent evolution.

Once typical spin and mass parameters of merging SMBHs are determined by *LISA*, either by direct measurement, or perhaps by extrapolating from detections at lower redshift,

combined with the event rate and what is known about the upper end of the mass function, this information is likely sufficient to give at least a strong indication on the typical SMBH growth rate and initial seed mass.

Our simulations above also confirm a result reported by Volonteri & Rees (2006), namely that SMBHs form primarily through repeated mergers of the most massive SMBHs merging with less-massive (SM)BHs. This is because the gravitational rocket speeds decrease rapidly as the mass ratio  $q$  decreases. The first few BHs that “outweigh” their neighbors – be it through being endowed with more mass at birth, accreting faster or being fortunate enough to survive the first mergers – will be less likely to be ejected from their host halos. This survival advantage becomes a runaway effect, as each subsequent merger will result in a lower value of  $q$  for the next merger.

### 3.2. Constraints on the SMBH Mass Function

Now that we have a first-glance grasp of the assembly parameters and their most basic observational characteristics, we can turn to identifying actual candidate models for the formation of  $m \gtrsim 10^9 M_\odot$  SMBHs before  $z \approx 6$ .

The suite of models discussed above has demonstrated that there are several feasible ways to build the SMBHs. These models have so far focused only on the number density of  $m \gtrsim 10^9 M_\odot$  SMBHs, and ignored indirect constraints that exist on the mass function at lower masses. In particular, the total mass density in SMBHs with masses in the range  $10^6 M_\odot \lesssim m \lesssim 10^9 M_\odot$  in the local Universe has been estimated by several authors, who find  $\sim 4 \times 10^5 M_\odot \text{ Mpc}^{-3}$  (to within a factor of  $\sim$ two; see, e.g., the recent paper by Shankar et al. 2009a and references therein). Furthermore, a comparison of the locally observed mass density with the mass density inferred from accretion by the evolving quasar population suggests that  $\sim 90\%$  of the total local SMBH mass density is attributable to quasar accretion. This implies that the total SMBH mass density increased by a factor of  $\sim 10$  between  $z \sim 6$  and the local Universe (Yu & Tremaine 2002, Haiman et al. 2004; Shankar et al. 2009a), which then places an indirect constraint on the SMBH mass function, down to  $m \sim 10^5 M_\odot$ , at  $z = 6$ .

To be specific, we set the following upper limit on the expected total  $z \approx 6$  SMBH mass density in  $m \gtrsim 10^5 M_\odot$  SMBHs:

$$\rho_{\text{SMBH},5+}(z = 6) \sim 0.1 \times \rho_{\text{SMBH},6+}(z \approx 0) \sim 4 \times 10^4 M_\odot \text{ Mpc}^{-3}, \quad (22)$$

That is, we assume that the total mass density of SMBHs with mass  $m > 10^5 M_\odot$  at  $z = 6$  is at most 10 percent of the total inferred mass density of SMBHs with mass  $m > 10^6 M_\odot$  in the

local universe. The major caveat to making such an expectation is that we assume that the low-mass end of the BH mass function has grown by a factor of 10, and that high-redshift quasar luminosity surveys have sufficiently accounted for selection effects of any SMBHs that may be hidden by inactivity or by being too dim.

The analysis that follows below is similar to that of Bromley et al. (2004), who considered the upper limit to the  $z \approx 6$  SMBH mass density in weighing the plausibility of various  $z = 6$  quasar BH assembly models. The main difference is that Bromley et al. (2004) did not consider the gravitational recoil effect. Adding in this recoil makes the problem significantly worse. This is because the recoil necessitates more optimistic assumptions in order to build up the  $\sim 10^9 M_\odot$  SMBHs, which tends to increase, by a large factor, the predicted number of lower-mass  $\sim 10^6 M_\odot$  SMBHs, which arise later, and whose growth is therefore less sensitive to the kicks. In other words, the kicks preferentially suppress the abundance of the most massive SMBHs which arise from the earliest seeds; as a consequence, we predict steeper SMBH mass functions than the models considered in Bromley et al. (2004). We performed a series of assembly calculations explicitly without recoil, and find that these indeed produce mass functions with a flatter slope and a higher normalization, owing to greater SMBH masses at the high-mass end, and a higher occupation fractions at all masses. If there are no kicks, less optimistic assumptions are required to produce the SDSS quasars, and the overall mass density is lower in no-kick scenarios that produce the minimum number of  $\gtrsim 10^9 M_\odot$  SMBHs.

The basic result we find is that among the models presented thus far, *all of those that match the SDSS abundance of the most massive SMBHs overshoot the above value by two or more orders of magnitude.* One possible solution to this apparent problem is that there is no problem at all: we have simply set our constraint too severely. Perhaps not all  $10^5 M_\odot$  SMBHs at  $z \approx 6$  have evolved to become  $m > 10^6 M_\odot$  BHs in galactic nuclei in the local universe. Still, there is no obvious way to “hide” these low-mass SMBHs locally, and the over-prediction in the SMBH densities in our simulations are very large: we find that in our fiducial models, we typically need to reduce the population of SMBHs in the mass range  $10^{5-7} M_\odot$  by a factor of  $\gtrsim 100$ , and those in the  $10^{7-9} M_\odot$  range by a factor of  $\gtrsim 10$ .

### 3.3. Successful Models I: BH Seeds Stop Forming Early

One logical solution, and one that has been suggested by Bromley et al. (2004), is to simply stop making seeds below some cutoff redshift. The earliest seeds contribute the majority of the total mass of the most massive SMBHs, and late-forming seeds tend to end up in lower-mass SMBHs. In principle, then, by introducing a cutoff redshift for seed

formation, one can suppress the low-mass end of the mass function, while still allowing for the formation of the most massive SMBHs. Such a model would also be in line with our physical understanding of seed BHs. We know Pop III stars stopped forming relatively early on in the universe, with the halt in production being due to trace metal contamination (e.g. Omukai et al. 2008), radiative feedback from the UV and/or X-ray background during the early stages of reionization (e.g. Haiman et al. 2000), the higher turbulence of gas in the centers of later halos, or a combination of these factors.

This proposed solution amounts to keeping  $f_{\text{duty}}$  a constant while allowing  $f_{\text{seed}}$  to evolve with  $z$ ; in the simplest case, as a step function dropping to  $f_{\text{seed}} = 0$  below some redshift. Figure 12 shows the fractional contribution  $(dM/dz_{\text{seed}})/M$  from seeds forming at different redshifts to the final mass at  $z = 6$  in three different bins of the  $z = 6$  SMBH mass function, for two different models that are marginally able to assemble the SMBHs powering J1054+1024. The model in the left panel has  $f_{\text{seed}} = 10^{-3}$ , while the model on the right has  $f_{\text{seed}} = 1$ . Note that contributions to each mass bin are normalized to integrate to unity, but the two lower mass bins  $\rho(10^{5-7}M_{\odot})$  and  $\rho(10^{7-9}M_{\odot})$  make up the vast majority of the total mass density. The formation epochs of the seeds contributing the majority of the mass of the different SMBHs are very distinct in the model with lower  $f_{\text{seed}}$ , but overlap significantly for  $f_{\text{seed}} = 1$ . What accounts for this qualitative difference in the assembly epochs? There are two ways to build  $10^9M_{\odot}$  holes: accretion onto the earliest-forming holes that undergo few mergers and grow mostly in isolation, and the mashed-together product of many seeds that may have formed later. If the occupation fraction is high, one expects both populations to contribute, and therefore a wide distribution for  $dM/dz_{\text{seed}}$ . If the occupation fraction is low, SMBHs with many progenitors contributing become rare, and we find that the most massive SMBHs can only be formed from isolated seeds in the earliest minihalos, through few mergers, and so the  $dM/dz$  curves in these models are sharply peaked.

Our task is to eliminate  $\approx 99\%$  of the BH mass in the lower-mass bins, while leaving most of the  $m \gtrsim 10^9M_{\odot}$  holes unaffected. By simply examining the normalized  $dM/dz$  curves in Figure 12, one can see that simply cutting off seed formation at an arbitrary redshift for the  $f_{\text{seed}} = 1$  model is not a viable solution to the overproduction problem, as there is no way to eliminate the lower-mass SMBHs without eliminating a significant fraction of the  $10^9M_{\odot}$  holes. Cutting off the seed production can produce successful mass functions for models with  $f_{\text{seed}} \ll 1$ , but only if the seed cutoff occurs at very high redshifts, typically  $z \sim 30$ . Essentially, the solution calls for a very brief and early period of seed BH formation, and very rare seed formation there after. An unfortunate generic consequence of this early cutoff redshift is that it quickly chokes off the *LISA* event rates.

We also simulated models where seed production continues beyond the cutoff redshift –

with the same probability  $f_{\text{seed}}$  as in the minihalos at  $z > z_{\text{cut}}$  – in halos with  $T_{\text{vir}} > 10^5\text{K}$ . Such halos could continue to form BHs if heating by the UV background is the primary mechanism for seed suppression, as they are able to shield their central gas from the UV radiation (Dijkstra et al. 2004). We find that models with such a partial cutoff overproduce the SMBH mass density if  $f_{\text{seed}} \gtrsim 10^{-4}$ . This result implies that either the initial occupation fraction is very low (it is still possible to make the SDSS BHs with this low  $f_{\text{seed}}$ ; see Table 2 below), or else some other feedback beyond UV radiation, such as metal–enrichment, stops seed BHs from forming in all halos at  $z < z_{\text{cut}}$ , even in the rare, more massive ones.

In short, the requirement in models in which the duty cycle is a constant, but seeds stop forming suddenly below some redshift, can be simply summarized as follows: the only way to build SMBH mass functions that satisfy observational constraints and indications at both the low-mass and the high-mass ends is from extremely rare seeds that form during a brief and very early epoch. We also note that these models are attractive because (i) there are physical reasons for the seeds to stop forming below some redshift, and (ii) there is independent empirical evidence, from constraints on the reionization history from *WMAP* measurements of the cosmic microwave background polarization anisotropies, that the ionizing luminosity in high–redshift minihalos was suppressed by a factor of  $\gtrsim 10$  (Haiman & Bryan 2006).

We present in Table 2 the parameters for four such successful models. While it is not computationally feasible to search the entire parameter space for such models, we present two typical examples for both the Pop–III–remnant and direct–collapse seed BH scenarios.  $f_{\text{seed}}$  is low in each of these examples, as we have argued above that they must be. Although we have listed the spin prescriptions, they are relatively unimportant because seeds are rare (see Section 3.1 above). Given a particular value for  $f_{\text{seed}}$ , the only free parameters are the accretion rate  $f_{\text{duty}}$  and the seed cutoff redshift  $z_{\text{cut}}$ . For the Pop III models, we find in the range  $f_{\text{seed}} \geq 10^{-4}$  that seeds must typically stop forming at  $z_{\text{cut}} > 30$ , with a lower cutoff  $z_{\text{cut}} \sim 20$  for the direct–collapse models. An important conclusion is that in each of these models, GW events are too rare ( $< 10^{-3}/dz/yr$  for  $z < 30$ ) for *LISA* detections beyond  $z \sim 6$  to occur within the mission’s lifetime.

The mass density of *ejected* BHs is exceedingly low in each of the successful scenarios,  $< 10^{-3}M_{\odot} \text{Mpc}^{-3}$ . Because the total number of seeds is small, so are the number of ejected holes. We only give an upper limit here, because the ejected holes are too rare for us to give a robust value given the statistical limitations of our “halo cloning” method for populating the entire halo population at  $z = 6$  (the mass density in ejected BHs can be large in models with large  $f_{\text{seed}}$ ; see below).

These models represent the simplest scenarios for SMBH formation, requiring a very brief period of seed formation and a prolonged period of accretion at rates comparable to



the Eddington rate, and consequentially they represent the most pessimistic predictions for *LISA*'s observational prospects.

### 3.4. Successful Models II: Feedback Adjusted to Maintain $m$ - $\sigma$ Relation

While the suppression of BH seed formation is an attractive possibility that fits constraints on the  $z = 6$  SMBH mass function, it is clearly not unique. One alternative solution to the over-production problem is to simply reduce the accretion rate of lower-mass BHs at lower redshifts. This is again physically plausible: accretion could be choked off as a result of the baryonic gas being churned into stars, being heated and dispersed by reionization feedback, or through self-induced negative feedback where the BH's own accretion-powered radiation stops the gas supply. Rather than try to model such a time- (and probably mass-) dependent mass accretion scenario, we examined several model variants, in which BHs are allowed to accrete just enough mass to match the value inferred by the  $m$ - $\sigma$  relation between BH mass and host halo velocity dispersion. That is, at each timestep  $t \rightarrow t + \Delta t$ , all BHs were assumed to grow in mass by  $m \rightarrow m + \Delta m$  such that the  $m - M$  relation is satisfied at the new host halo mass and redshift. However, whenever this requires super-Eddington growth, i.e. if  $(m + \Delta m)/m > \exp(\Delta t/t_{\text{Edd}})$ , then Eddington growth is applied instead. The main additional assumption here is that the  $m$ - $\sigma$  relation remains valid at all redshifts (which is at least consistent with a comparison between the evolution of quasars and early-type galaxies at  $0 < z \lesssim 6$ ; Haiman et al. 2007; Shankar et al. 2009b). As above, we adopt Equation (20) as our extrapolated  $m/M$  relation.

The BHs in these models form as  $100M_{\odot}$  seeds, and, given their host halo mass and redshift, accrete to match this relation as closely as possible without exceeding the Eddington accretion rate. If the simulation completes with the mean BH accretion rate well below the Eddington rate at all redshifts, then it is consistent with satisfying the Eddington accretion rate and the  $m - M$  relation inferred by Equation (20). As we shall find below, in our models the maintenance of the  $m$ - $\sigma$  relation does not typically require that the Eddington accretion rate is saturated (see Figure 15 below) as long as the  $f_{\text{seed}} \gtrsim 10^{-2}$ . If both the seed mass and the seeding fraction are low, it is increasingly difficult to satisfy Equation (20) at higher redshifts while simultaneously satisfying the Eddington upper limit. We find that for  $f_{\text{seed}} \lesssim 10^{-2}$ , accretion must saturate at the Eddington rate for much of  $z \gtrsim 15$  until the extrapolated  $m$ - $\sigma$  relation is satisfied, with the mass function falling below this relation at earlier stages of growth.

Recoil velocities are calculated with the spin magnitudes chosen uniformly between 0.0 and 0.9. As with our previous models, we run simulations where the spins are either randomly

oriented or completely aligned with the angular momentum vector of the binary orbit. This class of models in effect represents the most optimistic *LISA* expectations, as it allows us to keep numerous seeds, while simply adjusting the accretion rate, as described above, to keep the mass function within bounds. Note that the recoil speeds are also minimized by our choice for the spin alignment.

We show the mass functions and occupation fractions for this model in Figure 13, for three different values of the cutoff redshift below which new seeds are not formed,  $z_{\text{cut}} = 0, 12$  and  $18$ . Note that it is still possible to form the SDSS quasar-SMBHs via Eddington-limited accretion by  $z \approx 6$  even if seeds form in just 0.1% of all 1200K halos and only before  $z = 18$ . We do not plot the  $m/M$  relation, as it is satisfied in the form of Equation (20) in all cases shown here, by construction. These models also satisfy, by construction, the upper limit for the SMBH mass density. In all of the models shown in Figure 13,  $\rho_{\text{SMBH},5+}(z = 6) \gtrsim 1.3 \times 10^4 M_{\odot} \text{ Mpc}^{-3}$  if  $f_{\text{seed}} \geq 10^{-2}$ . In the  $f_{\text{seed}} = 10^{-3}$  models, we find  $\rho_{\text{SMBH},5+}(z = 6) \sim 1.0 \times 10^4 M_{\odot} \text{ Mpc}^{-3}$ . The difference in  $\rho_{\text{SMBH}}$  is due to varying occupation fractions at the low end of the halo mass function. The mass functions in Figure 13 have a much shallower slope overall than those in Figures 5 and 8. For the mass functions shown earlier, the steeper slopes were due to the ratio  $m/M$  increasing with decreasing host halo mass; the observed  $m/M$  relation has the opposite trend.

We show the *LISA* event rates in these alternative models in Figure 14. Most significantly, we note that in the  $f_{\text{seed}} = 1$  versions of these successful models, the *LISA* event rate can be as high as  $30 \text{ yr}^{-1}$ . (Note that this number can be even higher if seeds can form in minihalos down to a virial temperature that is significantly lower than our assumed fiducial value of 1200K.) The rate is somewhat suppressed when compared to the earlier Pop III seed models (Figure 7) that exceeded realistic indications on the SMBH mass density, because the massive BHs in the *LISA* band are rarer due to the more modest growth rates. We draw the attention of the reader to the apparent independence of the detection rate on the seed fraction and seed formation cutoff in the cases where  $f_{\text{seed}} \gtrsim 10^{-1}$  and  $z_{\text{cut}} \lesssim 12$ . Because BH ejections probabilities are lower in these models when compared to the constant-accretion scenarios of Figures 7 and 10, and because the  $m/M$  ratios are the same function of  $M$  in all models shown, the *LISA* rates saturate and converge once the occupation fraction in the most massive halos approach unity. Because the  $T = 1200\text{K}$  halos form in greatest abundance at  $z \sim 20$ , the  $z_{\text{cut}} = 12$  case hardly differs from the case with no seed cutoff.

A key characteristic of any SMBH assembly scenario is the balance between growth through BH mergers and growth through gas accretion. As discussed above, the two must strike a balance such that they are able to account for the most massive observed quasar-SMBHs at  $z \sim 6$ , while also not exceeding the total observed SMBH mass density. In Table

3, we illustrate the relative importance of mergers *vs.* growth in the models presented in this paper: the four successful constant-accretion models from Table 2; two of the unsuccessful constant-accretion models, also in Table 2, which overproduce the universal SMBH mass density; and four of the models that explicitly follow the extrapolated  $m$ - $\sigma$  relation via Equation (20). The values shown in the table (in  $\log_{10}$ ) are the sum of the initial masses of all the seed BHs that enter our merger trees; the total mass of galactic BHs at  $z = 6$ <sup>5</sup>; and the total mass of BHs ejected before  $z = 6$ . We also calculate the ratio of the total (galactic and ejected) BH mass at  $z = 6$  to the total initial seed BH mass, which gives a simple measure of the growth through gas accretion. We see immediately the contrast between the two types of successful models: the constant-accretion scenario relies on gas accretion for much of the growth, typically several orders of magnitude in the total BH mass; where the self-regulating models essentially describe the most heavily merger-driven scenarios possible, requiring accretion-driven growth of as little as a factor of a few.

These models also produce a significant population of ejected BHs. Even though ejection rates are lower on the whole than our constant-accretion models (compared to the unsuccessful constant accretion Model X in Tables 2 and 3), two factors contribute to the ejected BH mass being comparable to the galactic BH mass at  $z = 6$ . First, seed BHs are allowed to be very common, especially in contrast to the successful constant-accretion Models A through D; this results in a far greater number of total merger events, and a high total number of ejections despite the lower ejection probabilities. Second, the surviving BHs do not grow nearly as rapidly in these models as in the constant-accretion scenarios, so that the ratio between the total galactic BH mass and the total ejected mass can remain low (whereas in the constant accretion scenarios, retained holes can rapidly outgrow their escaped counterparts.) In the  $f_{\text{seed}} = 1$  models, the ejected holes can outnumber and outweigh their retained galactic counterparts with mass densities of  $\sim 3 \times 10^4 M_{\odot} \text{ Mpc}^{-3}$  and number densities of  $\sim 100 \text{ Mpc}^{-3}$ . The mass function of the ejected holes is peaked slightly above the seed mass (because holes are most likely to be ejected at the earliest stages of their evolution, when their host halos are the least massive). All of the ejected BHs are  $\lesssim 10^4 M_{\odot}$  if spins are aligned, but in rare instances, SMBHs as massive as  $\sim 10^8 M_{\odot}$  are ejected in our models with randomly oriented spins (the ejected SMBHs with masses above  $m > 10^6 M_{\odot}$  have a very low number density, SMBHs of  $\sim 4 \times 10^{-5} \text{ Mpc}^{-3}$ , even in the model with the most ejections (random orientation, no cutoff redshift,  $f_{\text{seed}} = 1$ ).

---

<sup>5</sup>Note that the values in Table 3 include BHs of all masses equal to and above the seed mass, where we have considered only those with  $m \geq 10^5 M_{\odot}$  in computing the universal “SMBH” mass density in previous sections. Also note that we do not generate trees for DM halos with  $M(z = 6) < 10^8 M_{\odot}$ , and throughout this paper we do not account for any BHs that may reside in such halos.

These self-regulating accretion models work by adjusting the BH accretion rates according to the mass growth of their host halos. We plot the accretion rates in units of the Eddington rate for this new set of models in Figure 15. We do so for the  $z_{\text{cut}} = 12$  case with four combinations for  $f_{\text{seed}}$  and spin alignment, and for three different BH mass ranges:  $10^3 M_{\odot} \leq m \leq 10^6 M_{\odot}$ ,  $10^6 M_{\odot} \leq m \leq 10^8 M_{\odot}$ , and  $m \geq 10^8 M_{\odot}$ . Note that the accretion rates must be slightly higher if BH binary spins are randomly oriented, in order to compensate for the higher ejection rates. Similarly, accretion rates are higher if seeds are less common, in order to compensate for the reduced merger-driven growth. For the models shown, the duty cycle (the mean accretion rate in Eddington units) for the most massive SMBHs converge to  $\sim 0.2$  at  $z \approx 6$ , though it can be as high as  $\gtrsim 0.5$  at  $z \gtrsim 8$  if merger-driven growth is hindered by low occupation fraction or recoil-induced ejections.

We note that similar merger–tree models tracking SMBH growth have been published. For example, Koushiappas et al. (2004) presented a similar model where the SMBHs are assembled primarily through mergers of directly-collapsed halo cores. Bromley et al. (2004) also presented SMBH assembly model wherein gas accretion activity was triggered by major mergers of the BHs’ host halos; in their model, a set fraction of the baryonic mass of the host was fed to the BH at each major merger. Their prescription (albeit without gravitational recoil) successfully produced the most massive SDSS SMBHs before redshift  $z = 6$  without overproducing the mass density. In general, this type of assembly model is fairly easily tuned to broadly reproduce the  $m - \sigma$  relation, as the parallel mass growth of BHs and their host halos is built in.

#### 4. Conclusions

In this paper, we have attempted to map out plausible ways to assemble the  $\gtrsim 10^9 M_{\odot}$  SMBHs that power the bright redshift  $z \approx 6$  quasars observed in the SDSS, without overproducing the mass density in lower–mass ( $\sim 10^{5-7} M_{\odot}$ ) BHs. We also computed the event rates expected for *LISA* in each of the successful models.

The physical effects governing SMBH assembly depend on the answers to four basic questions: (1) how common are the initial BH seeds; (2) how much mass in gas do they accrete, and therefore how much they contribute individually to the final SMBH’s mass; (3) how often do they merge; and (4) what happens to SMBH binaries when they do merge? Currently, we do not have empirical constraints to offer definitive answers to any of these questions. However, we are capable of predicting the final outcome, starting with a set of assumptions for the underlying physics. Our trees-plus-orbits algorithm simulates the formation history of SMBHs and the subsequent detection rate expectations for *LISA* by

isolating and prescribing answers to the above four questions. It is a powerful simulation tool, as it can incorporate a detailed modeling of individual physical prescriptions without a significant increase in the computational load, as long as the prescriptions can be described by fitting formulae, tabulated in a lookup table of reasonable size or summarized in a statistical manner.

Using this tool, we have surveyed a wide range of candidate assembly models, and reported on common and distinguishing traits in the resulting SMBH mass functions and the corresponding *LISA* detection rates. In particular, we have shown that SMBHs can form in a manner consistent with other observational evidence either through the rapid growth of rare, massive seeds, or through ultra-early production of numerous Pop-III remnant seeds, provided these seeds stop forming below a redshift  $z_{\text{cut}} \sim 20 - 30$ . We reach the pessimistic conclusion that these scenarios do not produce *any* detectable *LISA* events at  $z > 6$  (at least not in a few year’s operation). An alternative model, in which we assume that the extrapolation of the local  $m - M$  relation holds at all redshifts (e.g. due to internal feedback), on the other hand, can produce up to  $\sim 30$  *LISA* events per year, with a characteristic mass spectrum.

Our major findings can be summarized more specifically as follows:

- SMBHs must be continuously surrounded by dense gas that was able to cool at the centers of DM halos. Feeding holes with the low-density gas in DM halos whose gas was unable to cool does not allow for high enough accretion rates to explain the SDSS quasar BHs.
- If embedded in dense gas nearly continuously,  $\sim 100M_{\odot}$  seed BHs can grow into the SDSS quasar BHs without super-Eddington accretion, but only if they form in minihalos at  $z \gtrsim 30$  and subsequently accrete  $\gtrsim 60\%$  of the time. However, these optimistic assumptions, required to explain the SDSS quasar BHs, overproduce the mass density in lower-mass ( $\text{few} \times 10^5 M_{\odot} \lesssim M_{\text{bh}} \lesssim \text{few} \times 10^7 M_{\odot}$ ) BHs by a factor of  $10^2 - 10^3$ . We find that two conditions need to be satisfied to alleviate this overprediction: the initial occupation fraction of seed BHs has to be low ( $f_{\text{occ}} \lesssim 10^{-2}$ ), and new seeds must stop forming, or the seeds must accrete at severely diminished rates or duty cycles, at  $z \lesssim 20 - 30$ . We argued that models in which BH seeds stop forming at  $z \sim 20$  are attractive because there are physical reasons for the seeds to stop forming below some redshift (such as metal pollution and/or radiative feedback that suppresses pop-III star formation), and because there is independent empirical evidence, from *WMAP* constraints on the reionization history, that star and/or BH formation in high-redshift minihalos was suppressed by a factor of  $\gtrsim 10$  (Haiman & Bryan 2006).

- The simplest SMBH assembly scenarios, which have constant accretion rates, but in which BH seed formation stops abruptly at some redshift, and which meet constraints at both the high-mass and low-mass end of the  $z = 6$  SMBH mass function, predict negligibly low *LISA* event rates. The reason for the low rates is as follows: in these models, the BHs that grow into the most massive, highest-redshift quasar-SMBHs accrete at the same (exponential) rate as all the other BHs, typically resulting in a vast overproduction of massive ( $m \sim 10^6 M_\odot$ ) holes. In order to offset this overproduction, seeds must be made very rare, and this diminishes the *LISA* rates. It is difficult to envision a scenario for high ( $\gtrsim 10$  per year per unit redshift) detection rates unless a vast number of SMBHs in the  $10^{5-7} M_\odot$  range lurk in the universe at all redshifts, which the current electromagnetic surveys have missed.
- A different class of successful models, in which the SMBH masses are self-regulated by internal feedback, can evade this constraint, and produce *LISA* rates as high as  $30 \text{ yr}^{-1}$ . The key difference in these models that predict higher *LISA* rates is that the SMBH growth is driven by a large number of seed BHs and far lower gas accretion rates than those required in the constant-accretion models. The majority of these events occur at  $z \approx 6$  and in the low end ( $10^3 - 10^4 M_\odot$ ) of *LISA*'s mass range for detection. Also, for these models we find the ejected BH mass density can exceed that of the galactic BH population at  $z = 6$ . Most ejected holes are expected to have masses similar to the seed mass, but an ejected BH can be as massive as  $\sim 10^8 M_\odot$  if large recoil velocities are allowed (e.g. if spins are not always aligned with the orbital angular momentum of the binary).

In addition to the above, our modeling reveals a number of interesting aspects of SMBH assembly. We find that in the successful models the initial seeds are rare, and the most massive SMBHs grow primarily from the few 'lucky' early seeds that avoided ejection due to kicks. The precise assumptions regarding the kick velocity distribution (such as the assumed spin orientations or the resulting oscillation of the BH) tend to have only a modest effect on the final results in these models. This is because, at least in our simple prescription, BHs either return quickly to the gas-rich nucleus or are left wandering in the outer regions.

Our results suggest that *LISA* will be capable of narrowing the field of plausible SMBH assembly models from the raw event rate, even without detailed measurements of the binary spins or mass ratios. The spin and mass ratio measurements will further constrain the evolution of SMBH properties. While the component prescriptions explored in this paper are admittedly crude, exercises similar to the one performed in our study will be crucial in understanding the limits and possibilities offered by *LISA*, and ultimately to interpret the detected *LISA* events. The scarcity of empirical constraints on the various pieces of physics

that determines the SMBH growth leaves us with a large range of “plausible” scenarios and free parameters for SMBH assembly.

We thank Alessandra Buonanno for providing useful notes on the gravitational recoil effect, and Greg Bryan and Marta Volonteri for insightful conversations. We also thank Kristen Menou for helpful discussions and comments on the manuscript, and for providing invaluable computational resources. We also thank the anonymous referee for a report that helped improve this manuscript. This work was supported by NASA through the ATFP grant NNX08AH35G. ZH also acknowledges support by the Polányi Program of the Hungarian National Office of Technology.

## REFERENCES

- Abel, T., Bryan, G. L., & Norman, M. L. 2000, *ApJ*, 540, 39
- Abel, T., Bryan, G. L., & Norman, M. L. 2002, *Science* 295, 5552, 93
- Alvarez, M., Wise, J. H., & Abel, T. 2008, *ApJL*, submitted, preprint arXiv:0811.0820
- Arun, K.G., et al. 2008, in *Classical and Quantum Gravity*, special issue with contributions to the proceedings of 7th LISA Symposium, in press, gr-qc/0811.1011v1
- Baker, J.G., Centrella, J.; Choi, D.; Koppitz, M., & van Meter, J. 2006, *Phys. Rev. Lett.* 96, 111102
- Baker, J.G., Boggs, W.D., Centrella, J., Kelly, B.J., McWilliams, S.T., Miller, M.C., van Meter, J.R. 2008 *ApJ*, 682, L29
- Barkana, R. 2004, *MNRAS* 347, 57
- Barkana, R., & Loeb, A. 2001, *Physics Reports*, 349, 125
- Begelman, M., Volonteri, M., & Rees, M. J. 2006, *MNRAS*, 370, 289
- Berczik, P., Merritt, D., Spurzem, R., Bischof, H. 2006, *ApJ* 642, L21
- Berti, E., & Volonteri, M. 2008, *ApJ*, 684, 822B
- Binney, J., & Tremaine, S. 1988, *Galactic Dynamics*, Princeton University Press
- Blecha, L. & Loeb, A. 2008, *MNRAS*, 390, 1311

- Bogdanovic, T., Reynolds, C.S., Miller, M.C. 2007, ApJ 661L, 147B
- Bonning, E. W., Shields, G. A., & Salviander, S. 2007, ApJ 666, 13
- Boylan-Kolchin, M., Ma, C., Quataert, E. 2006, MNRAS 369, 1081
- Boylan-Kolchin, M., Ma, C., Quataert, E. 2008, MNRAS 383, 93
- Bromley, J.M., Somerville, R.S., & Fabian, A.C. 2004, MNRAS 350, 456
- Bromm, V., Coppi, P. S., Larson, R. B. 2002, ApJ, 564, 23
- Bromm, V., & Loeb, A. 2003, ApJ, 596, 34
- Campanelli, M., Lousto. C., Marronetti, P., & Zlochower, Y. 2006, Phys. Rev. Lett. 96, 111101
- Cole, S., Lacey, C. G., Baugh, C. M., Frenk, C. S. 2000, MNRAS, 319, 168
- Dijkstra, M., Haiman, Z., Rees, M.J., Weinberg, D.H. 2004, ApJ 601, 2, 666D
- Eisenstein, D., & Hu, W. 1999, ApJ, 511, 5
- Escala, A., Larson, R., Coppi, P., & Mardones, D. 2004, ApJ 507, 765
- Fan, X., et al. 2001, ApJ 122, 2833
- Fan, X., et al. 2003, AJ 125, 1649
- Fan, X. 2006, New Astronomy Reviews, 50, 665
- Favata, M., Hughes, S.A., & Holz, D.E. 2004, ApJ, 607, L5
- Haehnelt, M. 2003, Class. Quantum Grav., 20, 31
- Ferrarese, L. & Merritt, D. 2000, ApJ, 539, L9
- Ferrarese, L. 2002, ApJ, 578, 90
- Gebhardt, K. et al. 2000, ApJ, 539, L13
- Guedes, J. Diemand, J. Zemp, M., Kuhlen M., Madau P., Mayer L., & Stadel, J. 2008, in Proceedings of the conference Galactic & Stellar Dynamics In the Era of High Resolution Surveys, 2008, AN, 329, 1004G
- Haiman, Z., Rees, M.J., & Loeb, A. 1997, ApJ, 476, 458H



- Haiman, Z., Rees, M.J., & Loeb, A. 1997, ApJ, 484, 985H
- Haiman, Z. 2004, ApJ 613, 36
- Haiman, Z. & Bryan, G. L. 2006, ApJ 650, 7
- Haiman, Z., Abel, T., & Rees, M. J. 2000, ApJ, 534, 11
- Haiman, Z., Ciotti, L, & Ostriker, J.P. 2004, ApJ 696, 763H
- Haiman, Z., Jimenez, R., & Bernardi, M. 2007, ApJ, 658, 721H
- Haiman, Z., & Loeb, A. 2001, ApJ 552, 459
- Haiman, Z., Thoul, A., Loeb, A. 1996 ApJ 464, 523
- Heger, A., et al. 2003, ApJ, 591, 288
- Hughes, S.A. 2002, MNRAS 331, 805
- Islam, R. R., Taylor, J. E., & Silk, J. 2004, MNRAS, 354, 629
- Keeton, C., Kuhlen, M., & Haiman, Z. 2005, ApJ 621, 559
- Kidder, L. E. 1995, Phys. Rev. D, 52, 821
- Komatsu, E. et al., 2008, ApJS, 180, 330K
- Komossa, S., Zhou, H., & Lu, H. 2008 ApJ, 678, L81
- Koushiappas, S.M., Bullock, J.S., Dekel, A., 2004 MNRAS 354, 292
- Koushiappas, S. M., & Zentner, A. R. 2006, ApJ, 639, 7
- Lacey, C., & Cole, S. 1993, MNRAS 262, 627
- Lang, R. & Hughes, S. A. 2006, Phys. Rev. D, 74, 122001; erratum 2007, Phys. Rev. D, 75, 089902
- Lippai, Z., Frei, Z., & Haiman, Z. 2008b, ApJL, 676L, 5L
- Lodato, G., & Natarajan, P. 2006, MNRAS, 371, 1813
- Machacek, M., Bryan, G., & Abel, T. 2001, ApJ 548, 509
- Madau, P., & Quataert, E. 2004, ApJ 606, L17

- Mayer, L., Kazantzidis, S., Madau, P., Colpi, M., Quinn, T., & Wadsley, J. 2007, *Sci* 316.1874M
- Menou, K. 2003, *Class. Quantum Grav.*, 20, 37
- Menou, K., & Haiman, Z. 2004, *ApJ*, 615, 130
- Menou, K., Haiman, Z., & Narayanan, V. K 2001, *ApJ*, 558, 535
- Mesinger, A., Bryan, G.L., & Haiman, Z. 2006, *ApJ*, 648, 835M
- Micic, M., Holley-Bockelmann, K., Sigurdsson, S. & Abel, T. 2007, *MNRAS*, 380, 1533M
- Milosavljevic, M., & Merritt, D. 2003, *ApJ* 596
- Navarro, J., Frenk, C., & White, S. 1997, *ApJ* 490, 493N
- Oh, S. P., & Haiman, Z. 2002, *ApJ*, 569, 558
- Omukai, K., Schneider, R., & Haiman, Z. 2008, *ApJ*, 686, 801
- O’Shea, B. & Norman, M. 2007, *ApJ* 654, 66
- Ostriker, E.C. 1999, *ApJ*, 513, 252O
- Press, W.H., & Schechter, P. 1974, *ApJ*, 187, 425P
- Pretorius, F. 2005, *Phys. Rev. Lett.* 95, 121101
- Richards, G. T., Strauss, M. A., Pindor, B., Haiman, Z., Fan, X., Eisenstein, D., et al. 2004, *AJ*, 127, 1305
- Schnittman, J., & Buonanno, A. 2007, *ApJ*, 662, 63
- Schnittman, J. D., Buonanno, A., van Meter, J. R., Baker, J. G., Boggs, W. D., Centrella, J., Kelly, B. J., & McWilliams, S. T. 2008, *Phys. Rev. D*, 77, 4031
- Sesana, A., Haardt, F., Madau, P. & Volonteri, M. 2004, *ApJ*, 611, 623
- Sesana, A., Haardt, F., Madau, P. & Volonteri, M. 2005, *ApJ*, 623, 23
- Sesana, A., Volonteri, M. & Haardt, F. 2007, *MNRAS*, 377, 1711S
- Shankar, F., Croce, M., Miralda-Escudé, J., Fosalba, P., & Weinberg, D. H. 2008b, *ApJ*, submitted, preprint arXiv:0810.4919

- Shankar, F., Weinberg, D. H., & Miralda-Escudé, J. 2009a, ApJ, 690, 20S
- Shankar, F., Bernardi, M., Haiman, Z. 2009b, ApJ, 694, 867S
- Shapiro, S. L. 2005, ApJ, 620, 59
- Shapiro, P. R., Ilyev, I., & Raga, A. C. 1999, MNRAS, 307, 203
- Shen, Y. et al. 2007, AJ, 133, 2222
- Somerville, R., & Kolatt, T. 2005, MNRAS 305, 1
- Spaans, M., & Silk, J. 2006, ApJ, 652, 902
- Turner, E.L. 1991AJ, 101, 5T
- Tegmark, M. et al. 1997, ApJ 474, 1
- Vecchio, A. 2004, Phys. Rev. D, 70, 042001
- Volonteri, M., Haardt, F., & Madau, P. 2003, ApJ 582, 559
- Volonteri, M., & Rees, M. J. 2005, ApJ, 633, 624
- Volonteri, M., & Rees, M. J. 2006, ApJ, 650, 669
- Willott, C.J., McLure, R.J., & Jarvis, M. 2003, ApJ 587L, 15W
- Willott, C.J., et al. 2006, NOAO Proposal 383W, ID #2006B-0383
- Whalen, D., Abel, T. & Norman, M. L. 2004, ApJ, 610, 14
- Wyithe, J. S., & Loeb A. 2003, ApJ, 590, 691
- Yoo, J., & Miralda-Escude, J. 2004, ApJ 614, L25
- Yoshida, N., Abel, T., Hernquist, L., & Sugiyama, N. 2003, ApJ, 592, 645
- Yoshida, N., Omukai, K., Hernquist, L. 2008, Science, 321, 669Y
- Yu, Q., & Tremaine, S. 2002, MNRAS 335, 965
- Zhang, J., Fakhouri, O., & Ma, C.-P. 2008, MNRAS, 389, 1521

Table 1: Masses and Quantities of Simulated DM Halos.

$M_{\text{lo}} < M < M_{\text{hi}}$	$\log_{10} N_{\text{bin}}$	$\log_{10} \langle M_{\text{bin}} \rangle$	$N_{\text{sim}}$	$W_{\text{bin}}$
$8.0 < \log_{10} M < 8.5$	12.33	8.22	50000	$4.28 \times 10^7$
$8.5 < \log_{10} M < 9.0$	11.78	8.72	27000	$2.23 \times 10^7$
$9.0 < \log_{10} M < 9.5$	11.20	9.22	15000	$1.06 \times 10^7$
$9.5 < \log_{10} M < 10.0$	10.57	9.71	9000	$4.13 \times 10^6$
$10.0 < \log_{10} M < 10.5$	9.87	10.2	5000	$1.48 \times 10^6$
$10.5 < \log_{10} M < 11.0$	9.08	10.7	2700	$4.45 \times 10^5$
$11.0 < \log_{10} M < 11.5$	8.14	11.2	1500	$9.20 \times 10^4$
$11.5 < \log_{10} M < 12.0$	6.98	11.7	900	$1.06 \times 10^4$
$12.00 < \log_{10} M < 12.5$	5.50	12.1	500	632
$12.50 < \log_{10} M < 12.85$	3.48	12.6	303	10.
$12.85 < \log_{10} M < \infty$	1.60	12.9	40	1.0

For each mass bin, BH assembly was simulated by creating a merger tree for  $N_{\text{sim}}$  Monte-Carlo halos, and the results were multiplied by the weighting factors  $W_{\text{bin}}$  to represent the Press-Schechter mass function for DM halos at  $z = 6$ .  $N_{\text{bin}} = \int_{M_{\text{lo}}}^{M_{\text{hi}}} dN/dM dM$  is the expected Press-Schechter number of halos in each bin, and  $\langle M_{\text{bin}} \rangle$  is the number-weighted mean halo mass in each bin.

Table 2: Properties of four successful (A-D) and two failed (X and Y) models for SMBH growth

Model	$m_{\text{seed}}$	$T_{\text{seed}}$	$f_{\text{seed}}$	$f_{\text{duty}}$	spin	$z_{\text{cut}}$	$\rho_{\text{SMBH},5+}(z = 6)$
A	$200M_{\odot}$	1200K	$10^{-4}$	1	aligned	25	$3.4 \times 10^4 M_{\odot} \text{ Mpc}^{-3}$
B	$100M_{\odot}$	1200K	$10^{-2}$	0.95	aligned	28	$5.1 \times 10^4 M_{\odot} \text{ Mpc}^{-3}$
C	$10^5 M_{\odot}$	$1.5 \times 10^4 \text{K}$	$10^{-4}$	0.6	random	13	$6.2 \times 10^4 M_{\odot} \text{ Mpc}^{-3}$
D	$2 \times 10^5 M_{\odot}$	$1.5 \times 10^4 \text{K}$	$10^{-2}$	0.55	aligned	18	$7.0 \times 10^4 M_{\odot} \text{ Mpc}^{-3}$
X	$100M_{\odot}$	1200K	1	0.8	random	0	$2.9 \times 10^8 M_{\odot} \text{ Mpc}^{-3}$
Y	$10^5 M_{\odot}$	$1.5 \times 10^4 \text{K}$	$10^{-3}$	0.6	aligned	0	$1.1 \times 10^6 M_{\odot} \text{ Mpc}^{-3}$

The above shows parameters for four models that (1) have constant accretion rates of  $f_{\text{duty}}$  times the Eddington rate; (2) produce by  $z = 6$  SMBHs massive enough to power the SDSS quasars; and (3) do not overproduce the overall SMBH population. In Models A and B the seed BHs are Pop III remnants, and in Models C and D the seeds are formed through direct-collapse in more massive halos. Models X and Y are unsuccessful models that barely produce the  $m \gtrsim 10^9 M_{\odot}$  SMBHs by  $z = 6$  but also far overproduce the lower-mass SMBHs.

Table 3: The total seed, total ejected, and total retained BH masses

Model	$m_{\text{seed, tot}}$	$m_{\text{GN}}(z = 6)$	$m_{\text{ejected, tot}}$	$m_{\text{BH, tot}}/m_{\text{seed, tot}}$
A	9.3	16.0	6.2	6.7
B	10.1	16.1	7.7	6.0
C	12.7	16.2	6.4	3.4
D	13.2	16.3	6.2	3.1
X	16.0	20.0	19.1	4.0
Y	14.6	17.5	12.7	2.9
$m\text{-}\sigma, z_{\text{cut}} = 0, f_{\text{seed}} = 1, \text{aligned}$	15.7	15.7	16.0	0.48
$m\text{-}\sigma, z_{\text{cut}} = 0, f_{\text{seed}} = 1, \text{random}$	15.7	15.7	16.3	0.70
$m\text{-}\sigma, z_{\text{cut}} = 0, f_{\text{seed}} = 10^{-2}, \text{aligned}$	13.7	15.6	12.9	1.9
$m\text{-}\sigma, z_{\text{cut}} = 18, f_{\text{seed}} = 1, \text{aligned}$	14.4	15.7	14.7	1.34

The decomposition of the final SMBH mass into the contributions from the initial stellar seed BHs and subsequent gas accretion. Masses are in  $\log_{10}$ , and in units of  $M_{\odot}$ . The columns, starting from the second and from left to right, show: the total initial seed mass; the total SMBH mass retained in nuclei at  $z = 6$ ; the total ejected BH mass, and  $\log_{10}$  of the ratio of the total (i.e. the sum of the ejected and nuclear)  $z = 6$  SMBH mass to the initial seed mass. The last ratio is a measure of the total growth due to gas accretion. The first four rows (A-D) show values for the four successful models. Also shown for comparison are values from two of the unsuccessful, constant-accretion models (X and Y) that overproduce the total BH mass function. The model parameters for Models A, B, C, D, X and Y can be found in Table 2. The models where the  $m\text{-}\sigma$  relation is enforced by hand can grow primarily through mergers, with gas accretion adding as little as a factor of a few to the total SMBH mass at  $z = 6$ . If  $f_{\text{seed}}$  is sufficiently high, they also eject a total mass in low-mass BHs that is comparable to the retained nuclear population (most of the ejected holes have a mass near the seed mass).

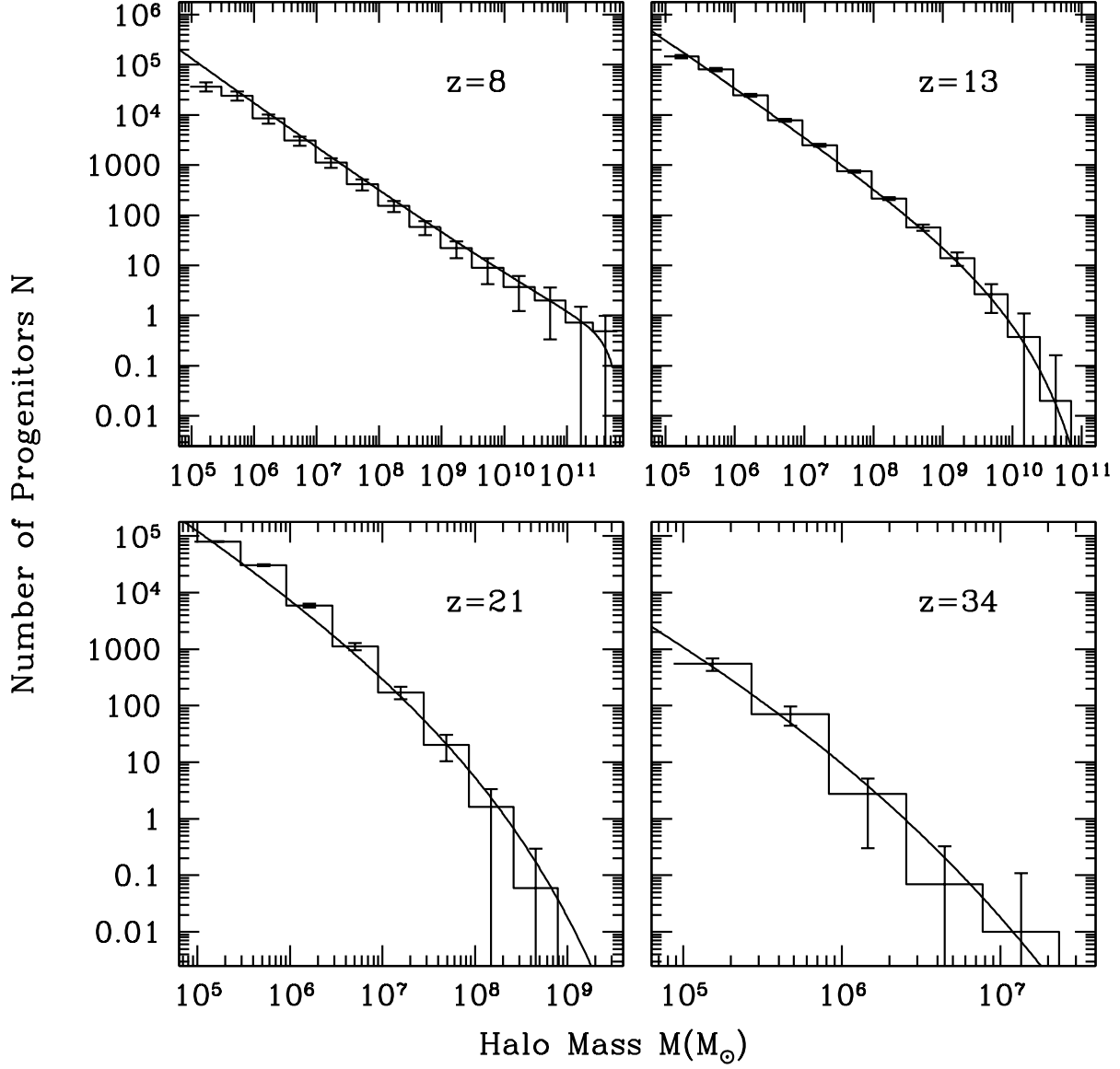


Fig. 1.— The Monte-Carlo-generated mass function of progenitors for a  $10^{12}M_{\odot}$ ,  $z_0 = 6$  parent halo at  $z = 8, 13, 21$  and  $34$ . The histogram is the mean number of 100 realizations, and the error bars demarcate the Poisson errors. The solid curve is the EPS prediction.

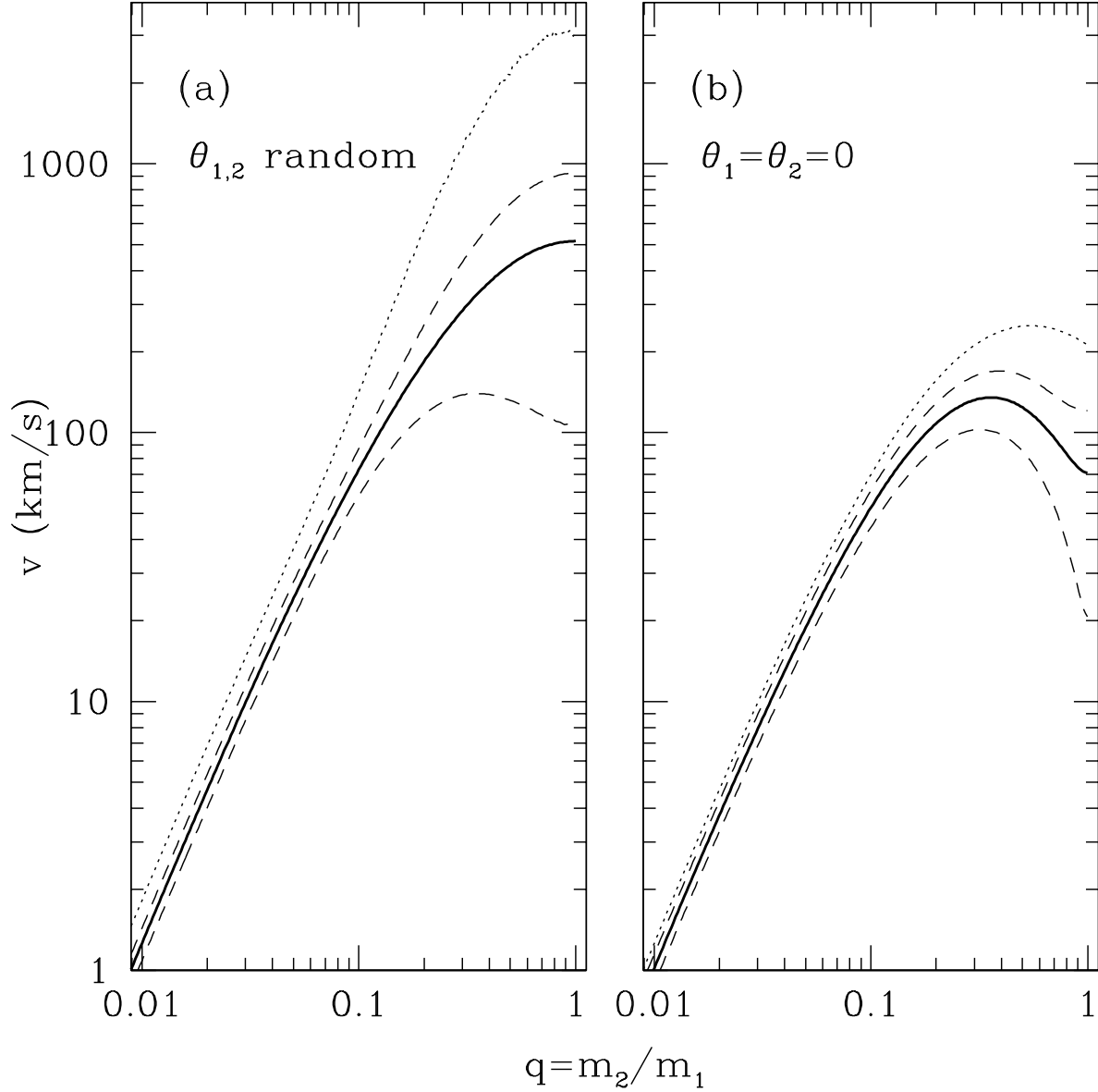


Fig. 2.— The kick velocity distribution as a function of the BH binary mass ratio, after  $10^6$  realizations of Equations (5-8) at each value of  $q$ . The left panel shows kicks for random spin orientations, while the right panel shows kicks when both BH spins are aligned with the orbital angular momentum. In each case, the spin magnitudes are chosen from a uniform random distribution in the range  $0.0 \leq a_{1,2} \leq 0.9$ . The solid curves show the mean, the dashed curves show the  $1\text{-}\sigma$  range, and the dotted curve gives the maximum value generated in the  $10^6$  realizations.

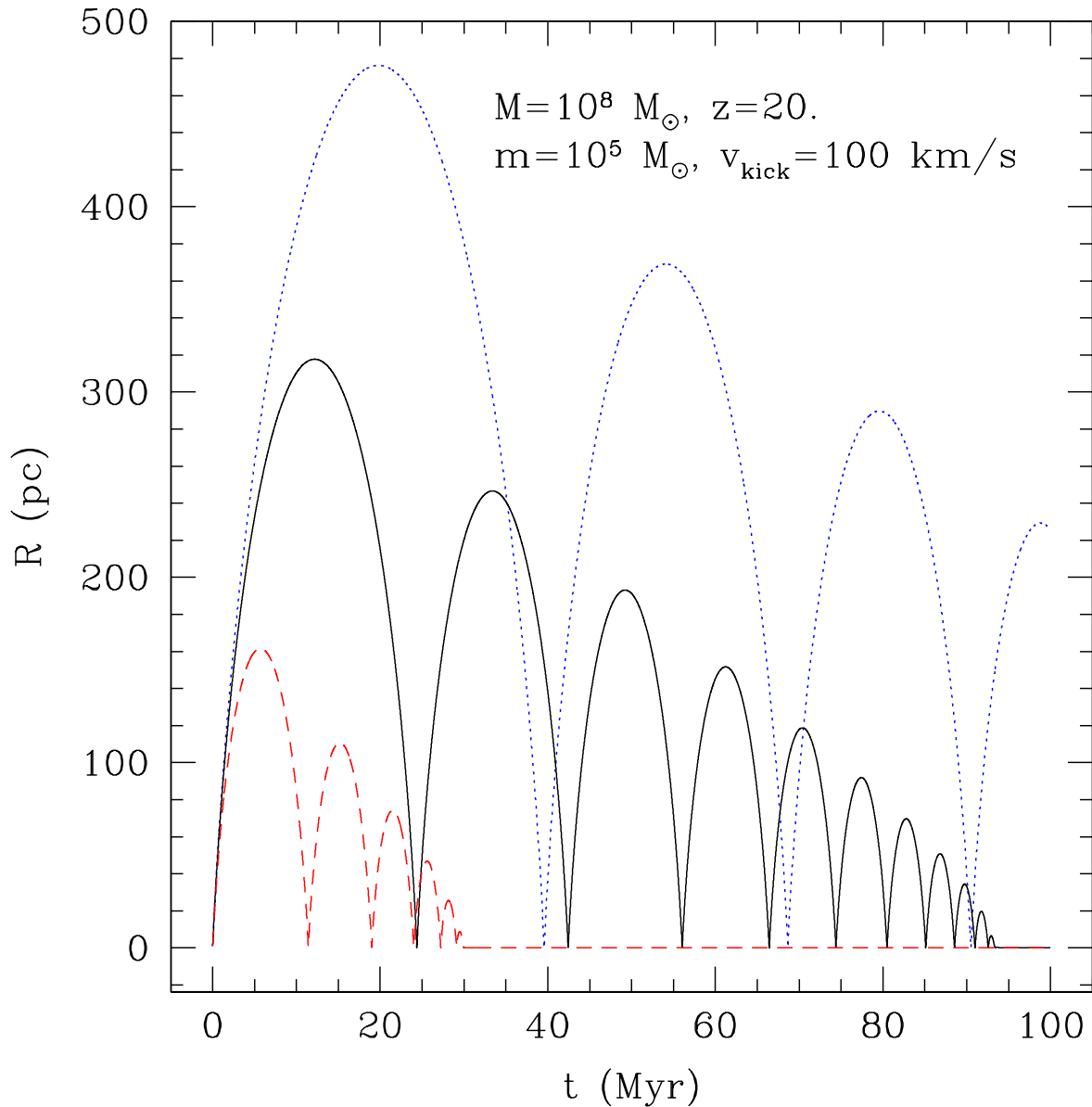


Fig. 3.— Examples of the radial motion of a recoiling black hole, for three different mass profiles for the host halo. The black curve shows the motion in a pure NFW halo; the halo of the blue (dotted) curve assumes that the host galaxy has a DM halo with an NFW profile and a corey gas component; the red (dashed) curve assumes a DM halo and a cuspy  $r^{-2.2}$  power law gas profile. In all cases, the halo mass is  $10^8 M_{\odot}$ , the BH mass is  $10^5 M_{\odot}$ , the redshift is  $z = 20$  and the kick velocity is  $100 \text{ km s}^{-1}$ .



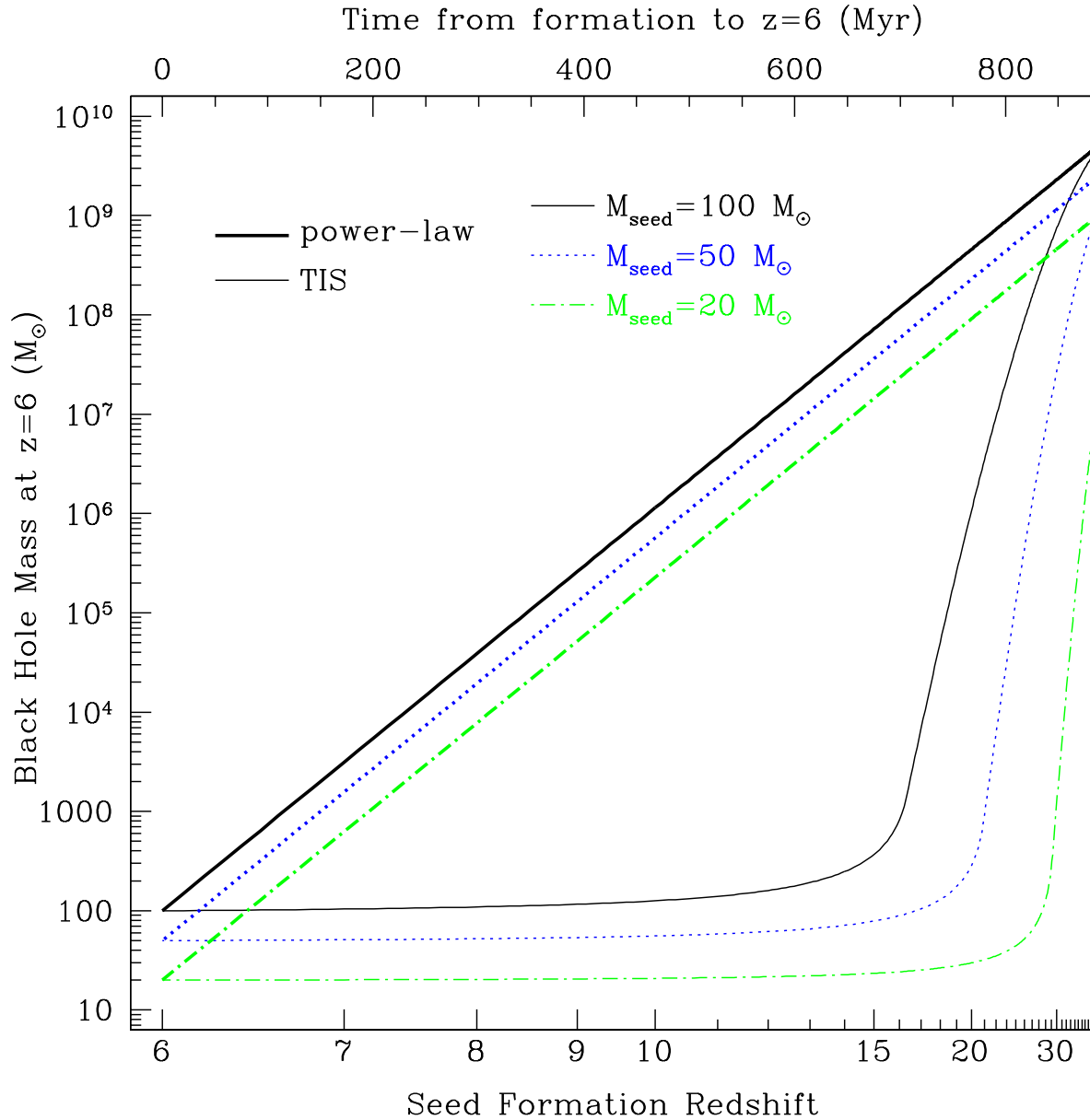


Fig. 4.— The maximum possible accreted mass by redshift  $z = 6$  for a seed BH born with a seed mass  $m_{\text{seed}}$  in a halo with virial temperature  $T_{\text{vir}} = 1200\text{K}$  at redshift  $z$ . If the BH is always surrounded by a steep gas profile, with a power-law cusp, the growth remains Eddington throughout (which appears as a straight line in this log-log plot). If the gas profile has a flat core (as in the TIS profile), the central density is initially insufficient to feed the BH at the Eddington rate, resulting in much slower growth. The cuspy and core gas distributions are demarcated by thick and thin lines, respectively, and different seed BH masses are shown in different colors (line styles).

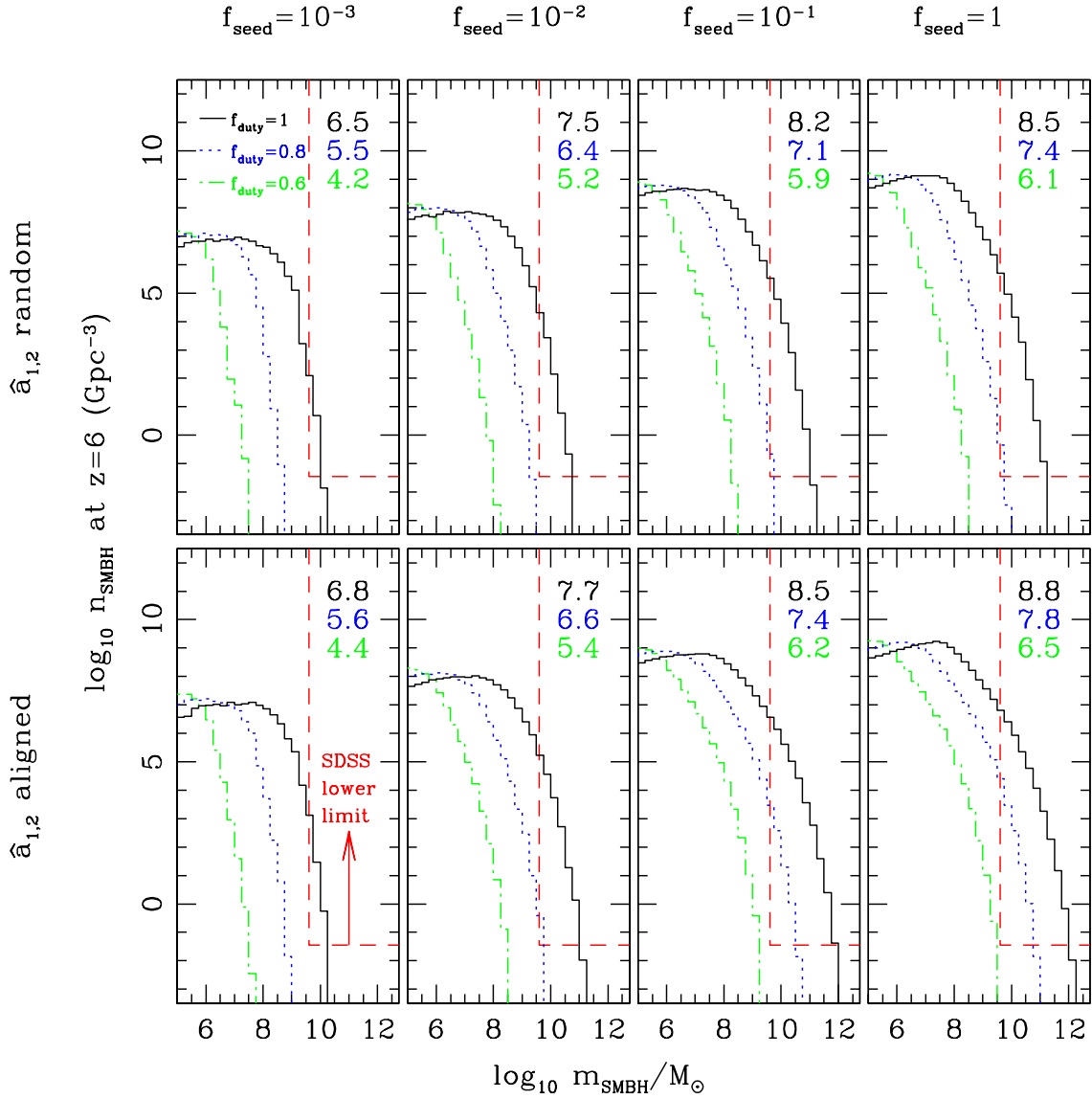


Fig. 5.— The comoving number densities of SMBHs in different mass bins at redshift  $z = 6$ . Colored figures are available in the online version. The 24 different models shown in the figure assume different parameter combinations as follows. The columns, from left to right, adopt  $f_{\text{seed}} = 10^{-3}, 10^{-2}, 10^{-1}, 1$ . The top row is for simulations with random binary spin orientation, and the bottom row is for spins aligned with the binary’s orbital angular momentum. Time-averaged accretion rates are distinguished by color: black (solid,  $f_{\text{duty}} = 1$ ), blue (dot,  $f_{\text{duty}} = 0.8$ ), and green (dash-dot,  $f_{\text{duty}} = 0.6$ ). The numbers in the upper-right corners represent  $\log_{10}[\rho_{\bullet} / (M_{\odot} \text{Mpc}^{-3})]$  for each model, in descending order of  $f_{\text{duty}}$ . The red (dashed) line demarcates the rough indication for the minimum number of  $z \approx 6$  SMBHs in the observable universe with  $m \gtrsim 10^{9.6} M_{\odot}$  given the area surveyed by SDSS.

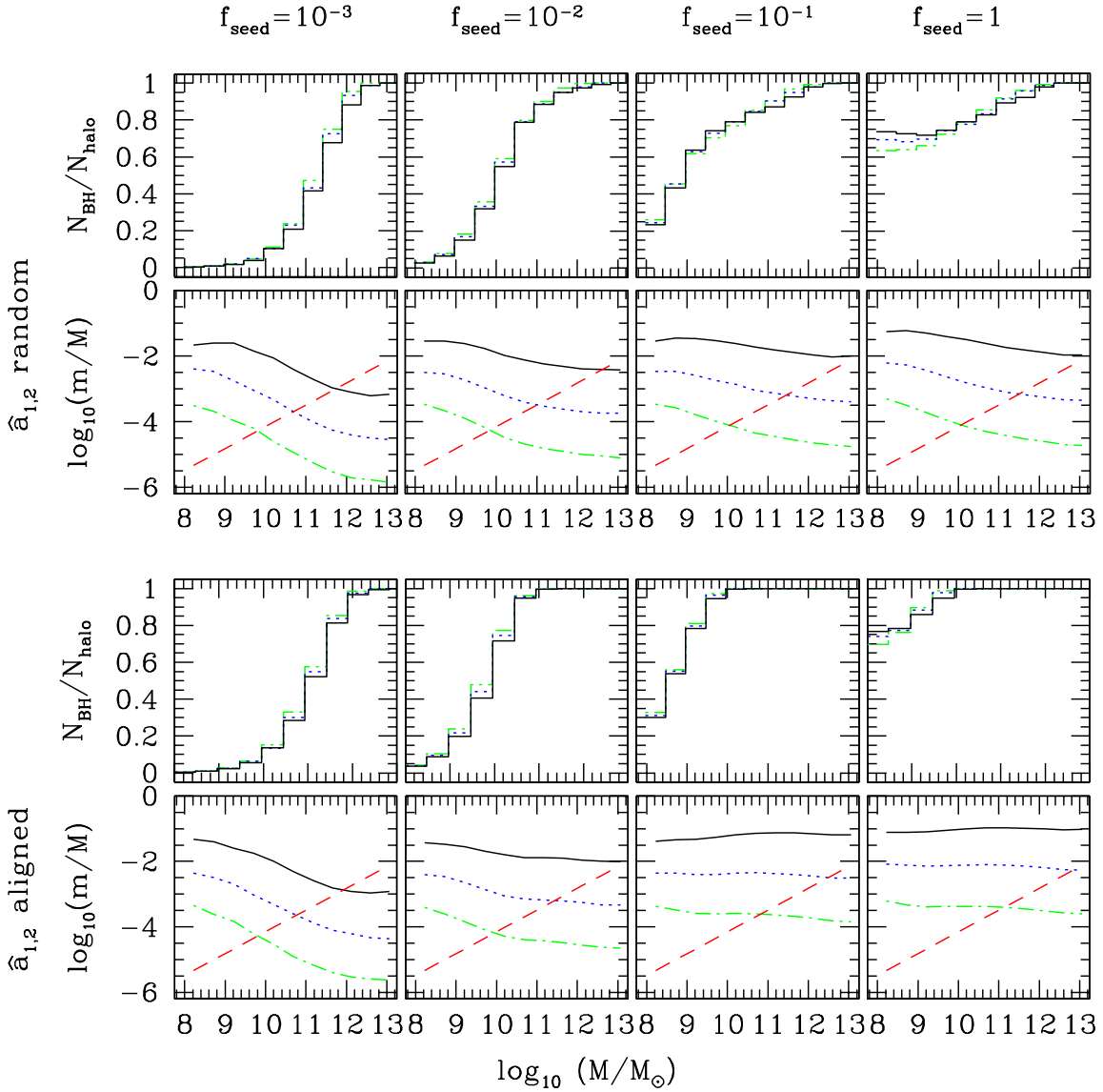


Fig. 6.— Properties of the SMBH population at  $z = 6$  as a function of the halo mass  $M$ : the percentage of DM halos hosting a central BH (assumed at most to be one BH per halo; top rows in both the upper and lower panels) with  $m \geq 10^{-5}M$ , and the mean BH-to-halo mass ratio  $m/M$  for the halos that do host a BH (bottom rows). Color (line-style) and panel schemes are the same as in Figure 5. The red (dashed) line is the empirical  $m/M$  relation extrapolated to  $z = 6$  (see Equation 20; Wyithe & Loeb 2003, Ferrarese 2002). Our  $m/M$  relation has the opposite trend with respect to halo mass from the trend observed in the local universe. Note that in some cases, the central BH consumes most of the baryonic mass in the halo.

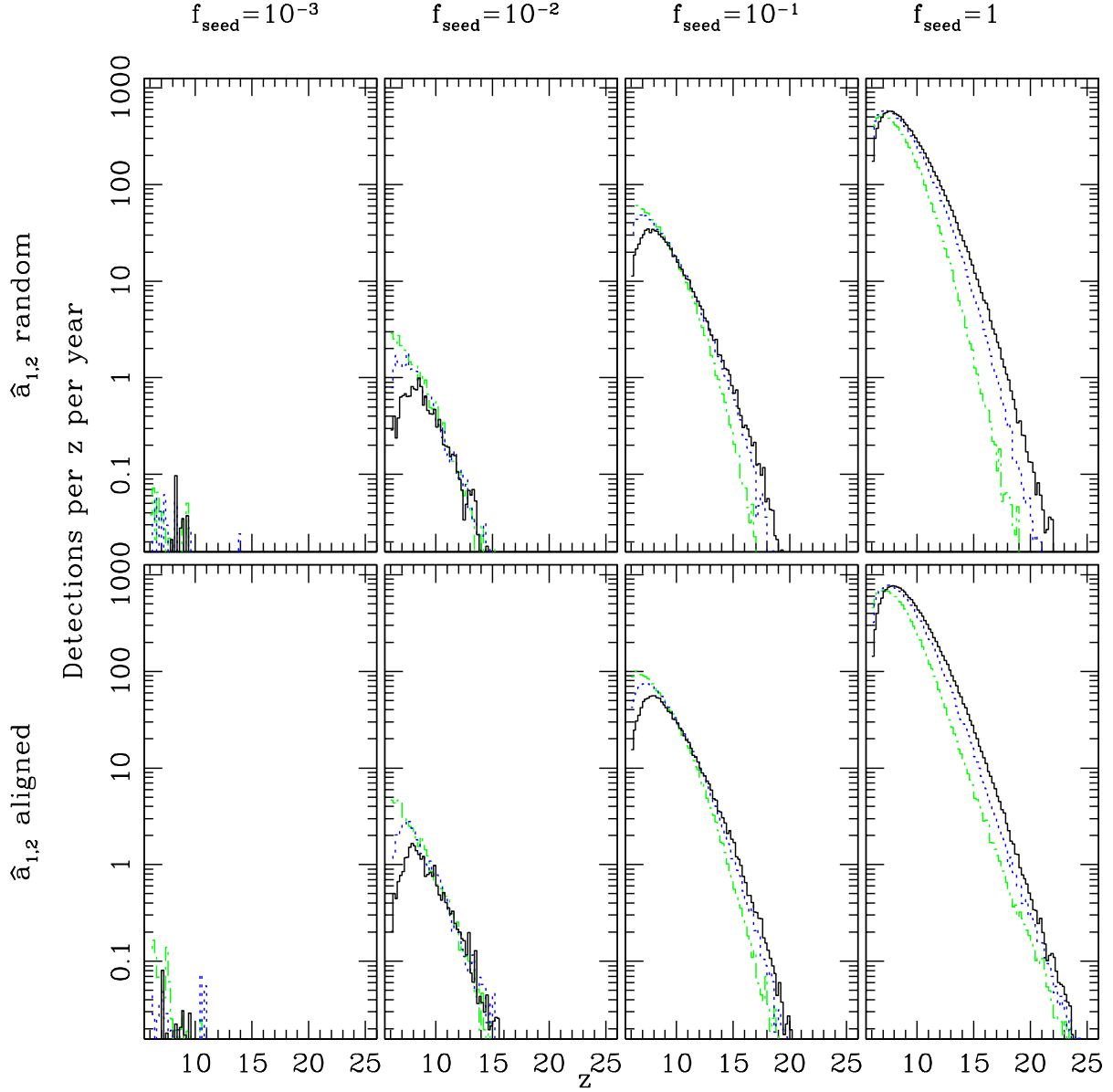


Fig. 7.— Expected number of *LISA* detections per redshift per year due to SMBH mergers with binary mass  $10^4 M_\odot \leq (m_1 + m_2)(1 + z) \leq 10^7 M_\odot$ . The color, line-type and panel schemes are the same as in Figures 5 and 6.

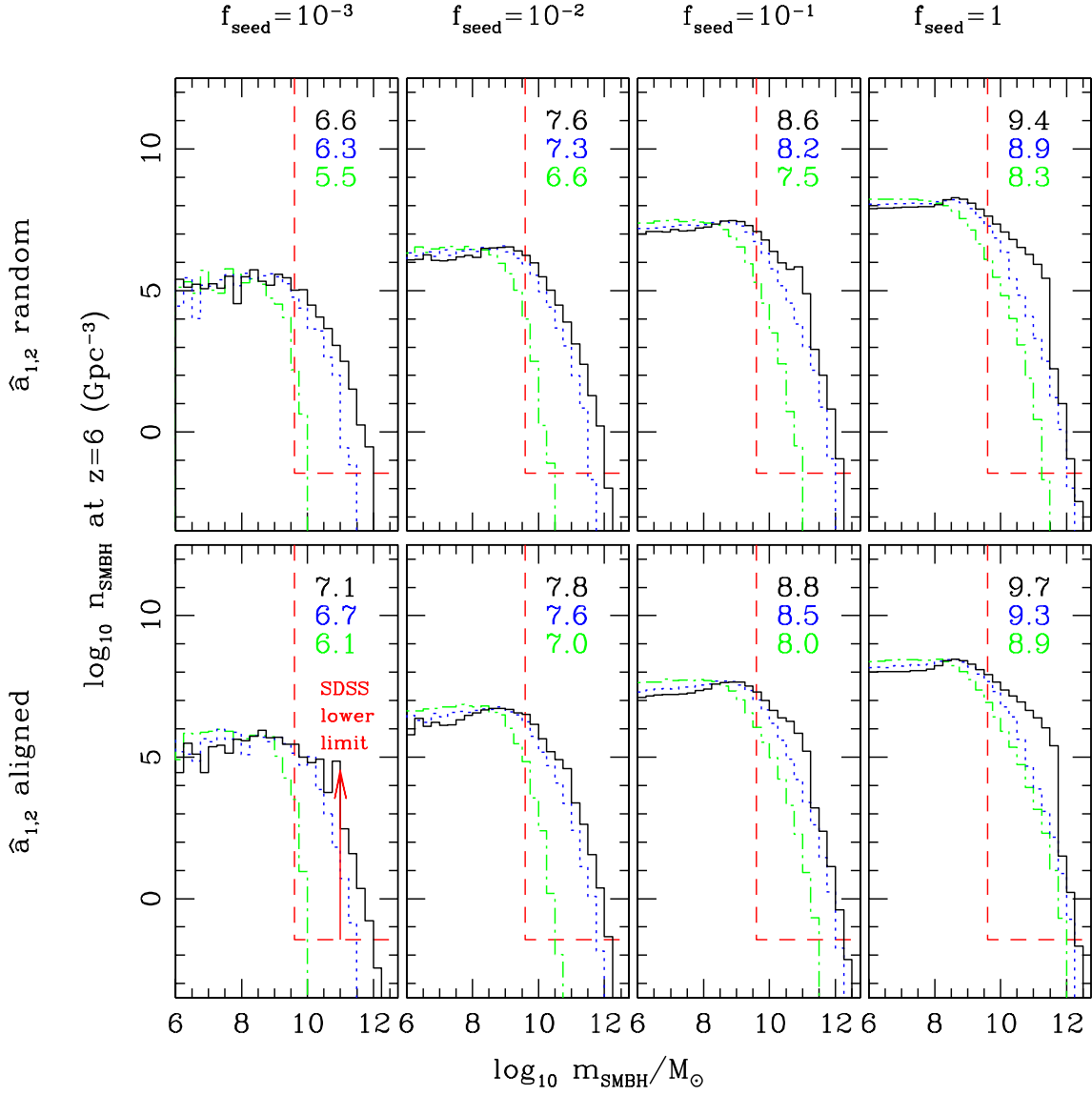


Fig. 8.— The  $z = 6$  SMBH mass function in the direct collapse scenarios, with  $m_{\text{seed}} = 10^4 M_{\odot}$  and  $T_{\text{seed}} = 1.5 \times 10^4 \text{K}$ . Color and panel organization for accretion rate, seed fraction and spin alignment is the same as in Figure 5.

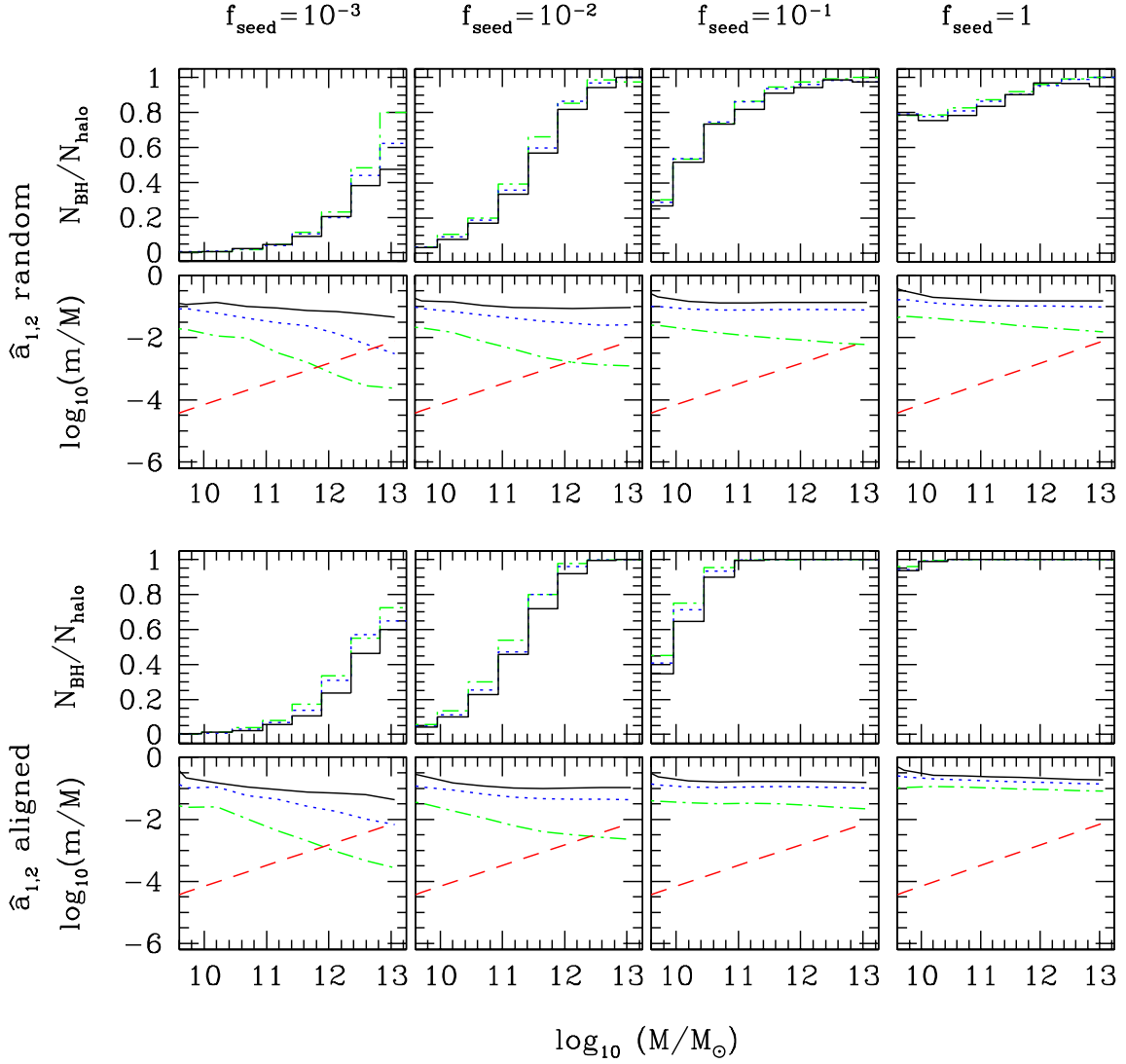


Fig. 9.— The SMBH occupation fraction and the  $m/M$  ratios in the direct collapse models. Refer to Figure 6 for color and panel organization. The dotted line is the extrapolated empirical  $m/M$  relation.

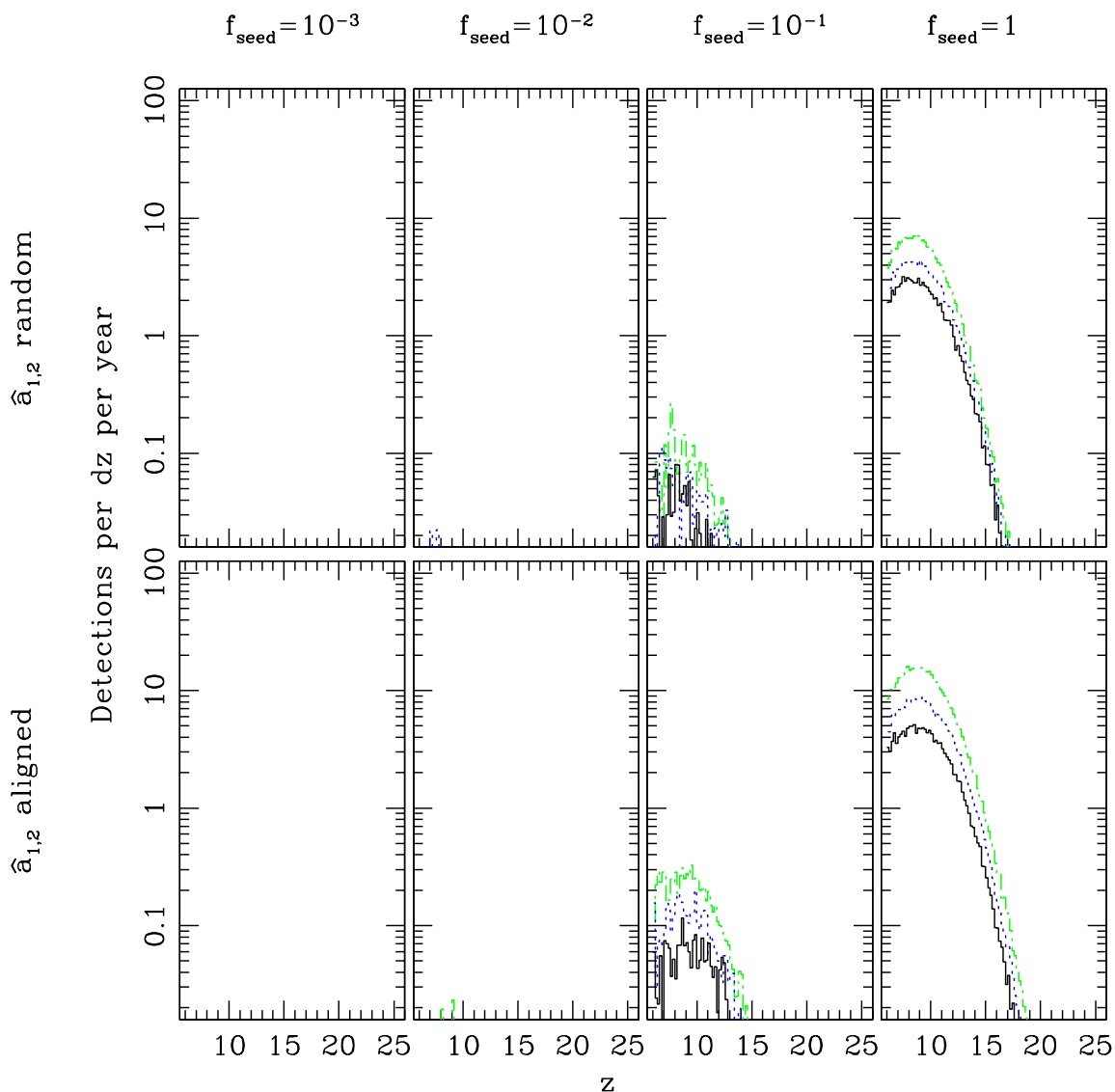


Fig. 10.— *LISA* event rates in the direct collapse scenarios. Refer to previous figures for color and panel organization. Note the significant reduction in the event rates relative to the pop-III seed models, owing to the smaller number of seed-forming halos in the tree.

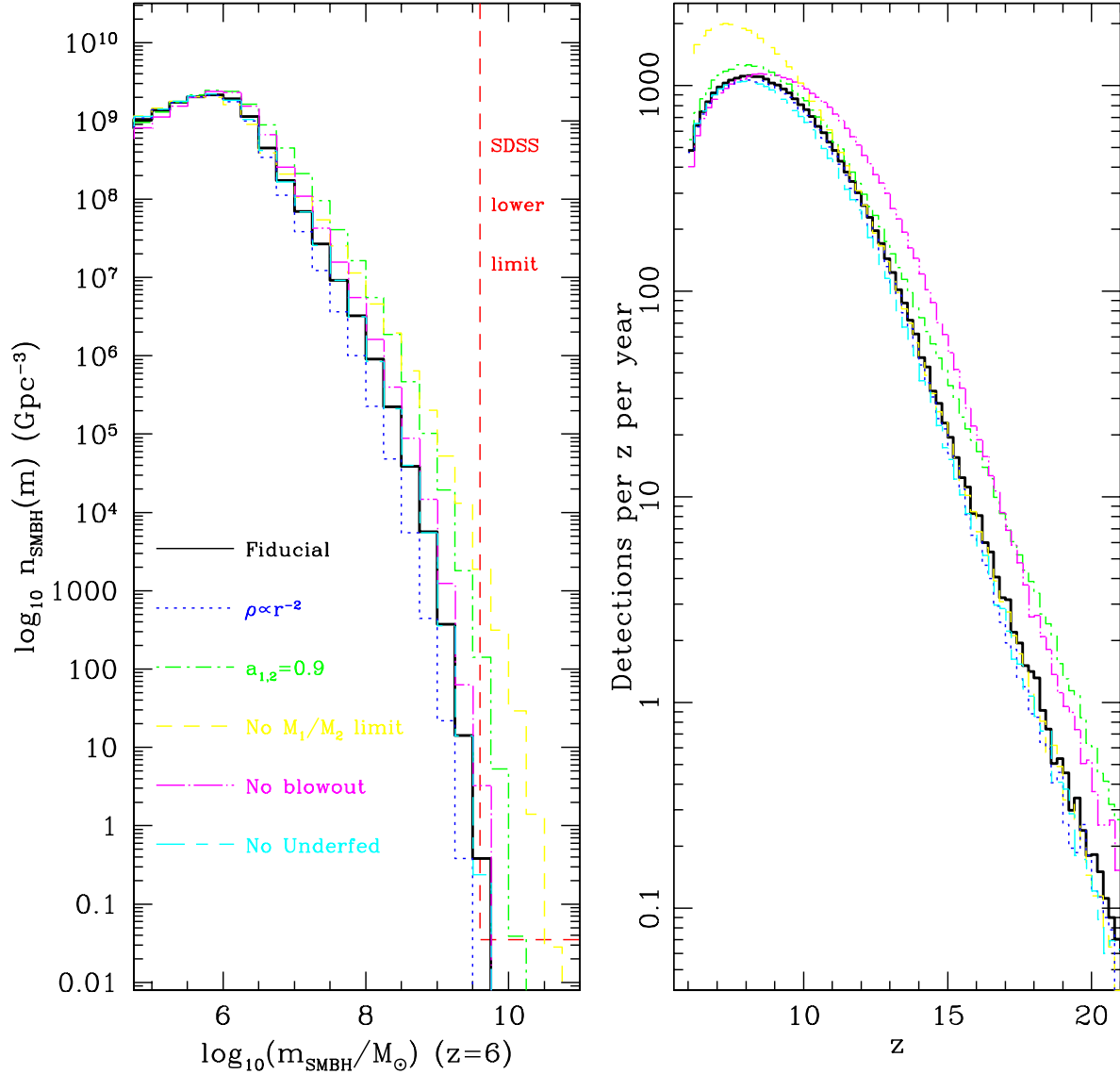


Fig. 11.— Properties of the SMBH population under several variants of our fiducial models. All models plotted have  $f_{\text{duty}} = 0.65$ ,  $f_{\text{seed}} = 1$ , and aligned binary spins, and modify a single aspect of the basic fiducial model prescription, as labeled: the gas density is an isothermal power-law instead of the fiducial  $\rho \propto r^{-2.2}$  (dark blue, dotted curve); spin magnitudes are near-maximal at  $a_{1,2} = 0.9$  (green, dot-short-dash curve); halos are allowed to merge and form BH binaries irrespective of their mass ratio (yellow, dashed curve); Pop III stars do not blow out the gas from their host halos prior to leaving a seed BH (magenta, dot-long-dash curve); and recoiling BHs wandering in low-density regions continue to accrete efficiently (light blue, long-short-dash curve). We also ran simulations with a corey, TIS gas profile for the host halos. We were unable to produce SMBHs of even  $\gtrsim 10^7 M_{\odot}$  in those models even when prescribing the most optimistic values for the other assembly parameters (therefore results from these models are not shown in the figure).



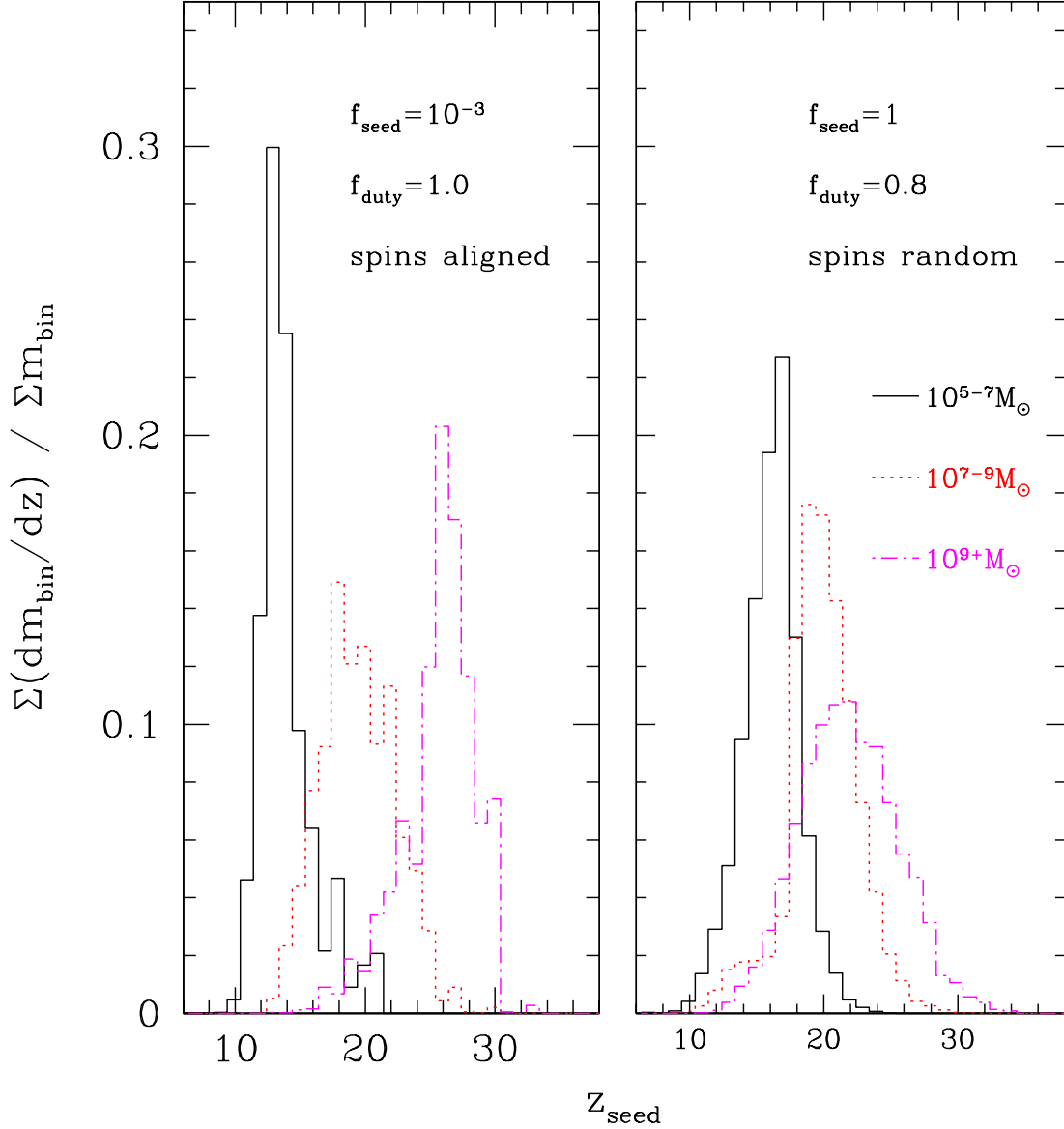


Fig. 12.— The fractional contribution to the mass of  $z = 6$  SMBHs from  $100M_{\odot}$  seed BHs that form at different redshifts  $z_{\text{seed}}$ . The contributions are computed in three mass bins of  $z = 6$  SMBHs:  $10^5 M_{\odot} \leq m < 10^7 M_{\odot}$  (black, solid lines),  $10^7 M_{\odot} \leq m < 10^9 M_{\odot}$  (red, dotted), and  $m \geq 10^9 M_{\odot}$  (magenta, dash-dot). The most massive  $z = 6$  SMBHs arise mainly from the earliest 1200K progenitors of the most massive halos ( $z \gtrsim 20$ ), whereas the seeds contributing most of the mass of lower-mass SMBHs formed later ( $z \lesssim 20$ ).

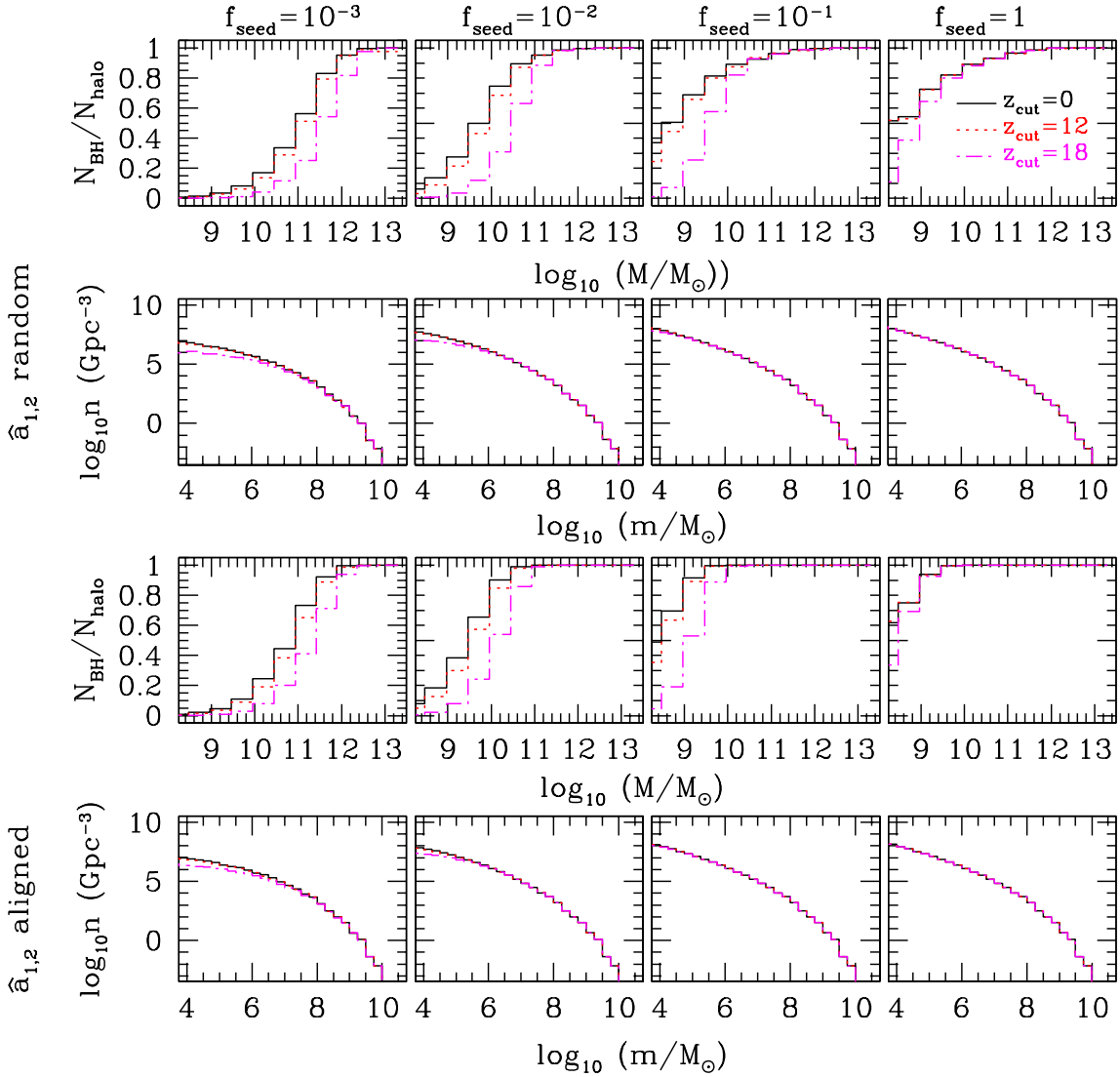


Fig. 13.— The SMBH mass functions and occupation fractions at  $z = 6$  for various models satisfying the  $m$ - $\sigma$  relation. These mass functions are much less steep in comparison to those shown in Figures 5 and 8. Occupation fractions are higher than those in Figures 6 and 9, as the BH binary mass ratios are generally lower compared to those models, resulting in less powerful recoil kicks.

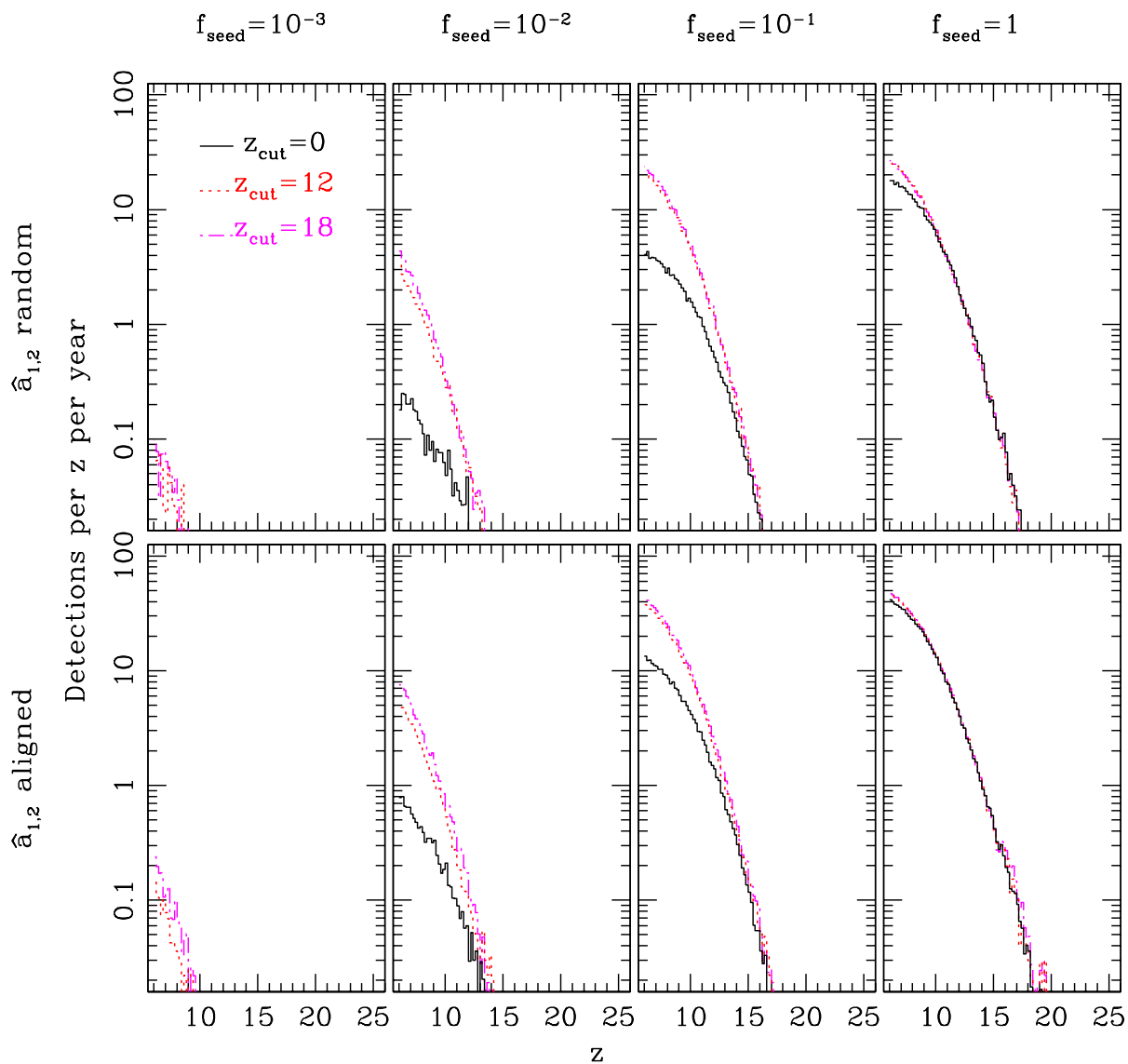


Fig. 14.— The *LISA* rates in models that satisfy the  $m$ - $\sigma$  relation at all redshifts as closely as possible without exceeding the Eddington accretion rate. Note that the rate saturates at  $30 \text{ yr}^{-1}$  at  $z \gtrsim 6$  for high seed fractions and low redshifts for seed cutoff.

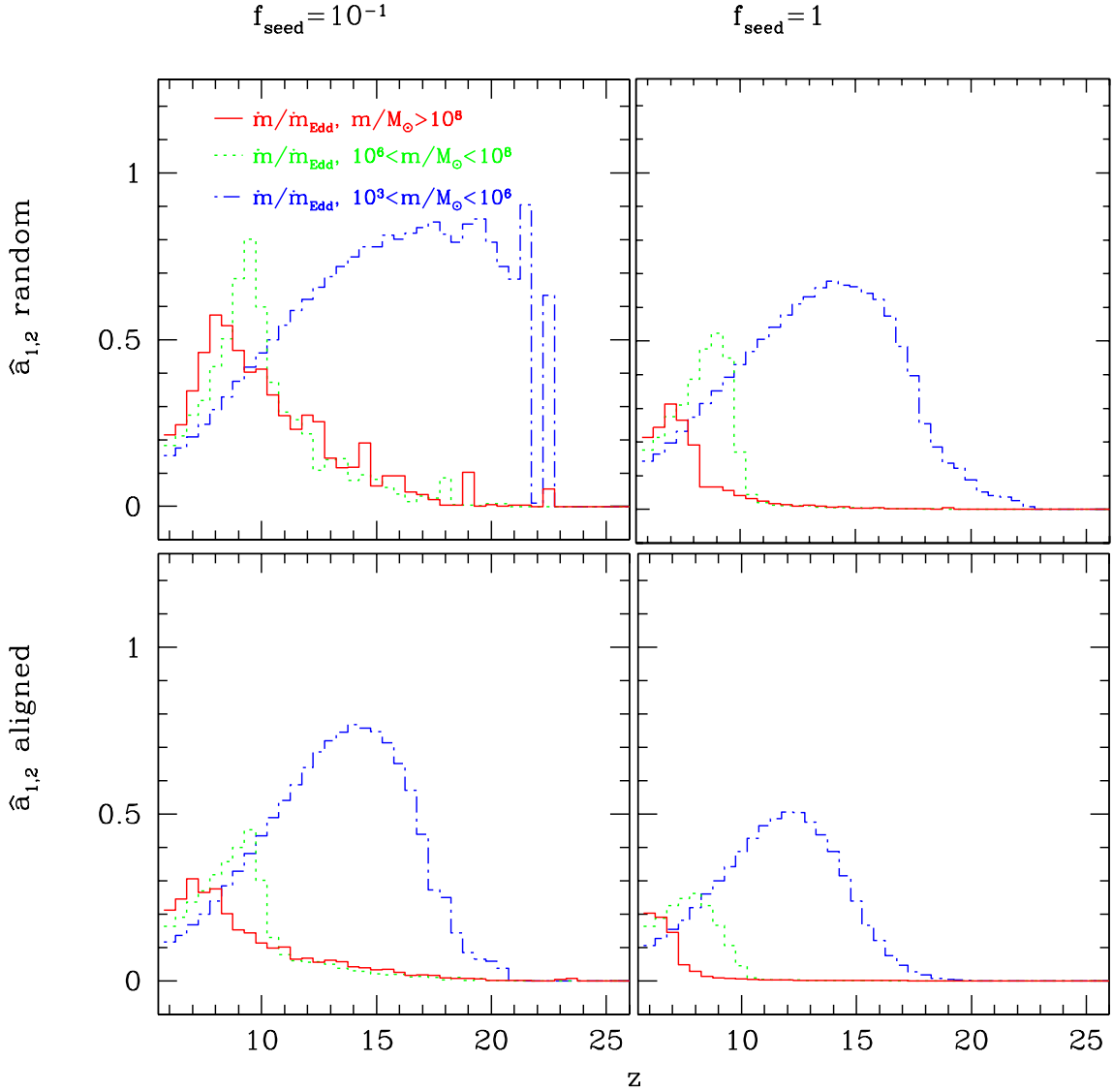


Fig. 15.— The accretion rate (thick lines) in Eddington limits in models that match the  $m$ - $\sigma$  relation (Equation 20) at all redshifts, for different ranges of BH masses. We also plot the merger rates (thin lines) in units of mergers per halo for different halo mass bins corresponding to  $M_1 + M_2 = 10^4 m$ . Note that masses are defined instantaneously at each redshift interval, rather than tracking the histories of the  $z = 6$  holes and halos.